Journal of Applied and Computational Mechanics, Vol. 3, No. 1, (2017), 37-59
DOI: 10.22055/jacm.2017.12619

Shahid Chamran University

Journal of
Applied and Computational Mechanics

Modeling of heat generations for different tool profiles in friction stir welding: study of tool geometry and contact conditions

M. A. Waheed[1], L. O. Jayesimi[2], S. O. Ismail[3], O. U. Dairo[4]

[1, 3] Department of Mechanical Engineering, Federal University of Agriculture, Abeokuta, Nigeria.
[2]Works and Physical Planning Department, University of Lagos, Akoka, Lagos, Nigeria.
[4]Department of Civil Engineering, Federal University of Agriculture, Abeokuta, Nigeria.

Received January 06 2017; revised February 11 2017; accepted for publication February 19 2017.
Corresponding author: L. Jayesimi, ljayesimi@unilag.edu.ng

Abstract

In this work, improved heat generation models are developed for straight and tapered shoulder geometries with different tool pin profiles in friction stir welding. The models are developed considering the welding process as a combination of the pure sliding and the pure sticking conditions. From the results, the amount of heat generation is directly proportional to the number of edges in the pin profiles in such a way that the heat generated in the profiles increases from the triangular pin profile to hexagonal pin profile. Also, increase in the tool rotational speed under constant weld speed increases the heat input while increase in the weld speed under constant tool rotational speed decreases the heat input and the rate of heat generation at the shoulder in a flat shoulder tool is more than that of conical/tapered shoulder tool. The predicted results show good agreements with the experimental results in literature.

Keywords: Frictional stir welding; Heat generation models; Different Tool Pin Profiles; Tool geometry; Contact Conditions.

1. Introduction

Friction stir welding (FSW) is a contemporary relatively efficient novel solid-state welding method invented at The Welding Institute (TWI) of UK in 1991. It is a remarkably simple welding technique in which non-consumable rotating tool with a specially designed pin and shoulder is inserted into the abutting edges of sheets or plates to be joined and traversed along the line of joint. It is considered to be the most significant development in metal joining in a decade and is a“green” technology due to its energy efficiency, environment friendliness, and versatility. Despite significant advances in the application of FSW and increasing usage as a relatively new joining technique for welding alloys, the fundamental knowledge of the thermal impact and thermomechanical processes of the technique are still not completely understood [1-4]. Without this knowledge, the process cannot be used to its full potential [2-4].

Research and development are progressing to explore the potentials of the welding process. Understanding the heat generation and the temperature history during the FSW process is the first step towards understanding the thermomechanical interaction taking place during the welding process. Modeling of heat generation during FSW can potentially accelerate the development of the welding process since the central issue in all cases is the determination of the heat input. In addressing the issue, several methods involving experimental analysis have been adopted to calibrate heat flow but none of these approaches enable the heat generation and weld temperature to be predicted without an experimental measurement of some kind. The determination of precise amount of heat generated during friction stir welding process is complicated since there are various uncertainties, assumptions and simplifications of mathematical model that describes welding process. Various experiments conducted around the planet, from the very beginning of the FSW method's application gave dispersive results about the generated heat. A more accurate and predictive approach uses the 3-dimensional flow field to calculate the heat generation from the material viscous dissipation. Even with the sophisticated models, there is conjecture over the best ways to describe the material behaviour and the interface between the workpiece material and the tool, i.e. is there stick or slip. The analytical heat generation estimate correlates with the experimental heat generation, by assuming either a sliding or a sticking condition. However, the main uncertainties about process are when welding condition is a mixture of sliding and sticking. In this situation ambiguity of the value of the friction coefficient in every moment of the welding process, contact pressure between weld tool and weld pieces and shear stress are main reasons for difference between analytical and experimental result. Understanding the process of heat generation and estimating the amount of heat generated during FSW are complex and challenging tasks that require a multidisciplinary approach. Therefore, the seemingly simple task of predicting the weld heat generation has proved beyond the ability of most models. Previous works on modeling the heat generation from the FSW tool are based on assumptions regarding the interface condition, which led some limitations and inaccuracies. In the model by Chao and Qi [5], heat generation model are developed based on the assumption of sliding friction, where Coulomb's law is used to estimate the shear or friction force at the interface. Also, in their model, the pressure at the tool interface is assumed to be constant, thereby enabling a radially dependent surface heat flux distribution as a representation of the friction heat generated by the tool shoulder, but neglecting the heat generated by the probe surface. Frigaard *et al.* [6] modeled the heat input from the tool shoulder and probe as fluxes on squared surfaces at the top and sectional planes on a three-dimensional model and control the maximum allowed temperature by adjustment of the friction coefficient at elevated temperatures. Russell and Shercliff [7] based the heat generation on a constant friction stress at the interface, equal to the shear yield stress at elevated temperature, which is set to 5% of the yield stress at room temperature. Gadash and Kumar [8] developed heat generation model for different pin profiles in friction stir welding considering only sliding condition while Colegrove [9] uses an advanced analytical estimation of the heat generation for tools with a threaded probe to estimate the heat generation distribution. The fraction of heat generated by the probe is estimated to be as high as 20%, which leads to the conclusion that the analytical estimated probe heat generation contribution is not negligible. Also, the real situation during the welding process is a combination of the pure sliding and the pure sticking [10]. Therefore, in this work, improved analytical models are developed for the predictions of heat generation in straight and tapered/conical shoulder profiles with triangular, square, pentagonal and hexagonal tool pin profiles in friction stir welding. The models are developed considering the welding process as a combination of the pure sliding and the pure sticking conditions.

2. Development of heat generation models for the friction stir welding

Consider the friction stir welding (FSW) shown schematically in Fig. 1. As pointed out previously, during the FSW, a rotating tool moves along the joint interface. As the tool moves along the joint and into the workpiece, heat generated at surface and near the interface between the tool and the workpiece is transported into the workpiece and the tool (Fig. 2). The total heat generated at different portions of the tool is the summation of the heat generated at the tool shoulder surface, heat generated at the tool pin/probe side and the heat generated at the tool pin/probe tip. Also, during the frictional stir welding, heat is generated by pure sliding (adhesion) and pure sticking (deformation). In pure sliding condition, it is assumed that there is shear in the contact interface and can be described as fully Coulomb friction condition. In the assumption, the contact pressure between tool and weld piece p and friction coefficient μ are constant or linearly dependable values from various variables. The shear stress becomes equals to dynamic contact shear stress. In the pure sticking, it is assumed shearing in the layer of the material of weld pieces very close to the contact surface and uniformity of the shear stress τ. In this situation, surface of the weld piece will stick to the moving tool's surface only if friction shear stress exceeds the yield shear stress of the weld piece. The real situation during welding process gives combination of the pure sliding and the pure sticking. Therefore, it is absolutely correct to say that heat generating during friction stir welding is mixture of pure sliding, pure sticking and combination of sliding and sticking [10].

As pointed in the previous works, the heat generated in FSW was considered to be due to friction (total sliding condition only), but practically, it is due to friction as well as deformation (sticking condition). Therefore, considering both types of heat and their influence on each other, the total amount of heat generated on the pin tip (*pt*), pin side (*ps*) and the shoulder tip (*st*) are respectively given by:

$$Q_{pt} = (1-\delta_{pt})Q_{pt}^{fr} + \delta_{pt}Q_{pt}^{def} \tag{1}$$

$$Q_{ps} = (1-\delta_{ps})Q_{ps}^{fr} + \delta_{ps}Q_{ps}^{def} \tag{2}$$

$$Q_{st} = (1-\delta_{st})Q_{st}^{fr} + \delta_{st}Q_{st}^{def} \tag{3}$$

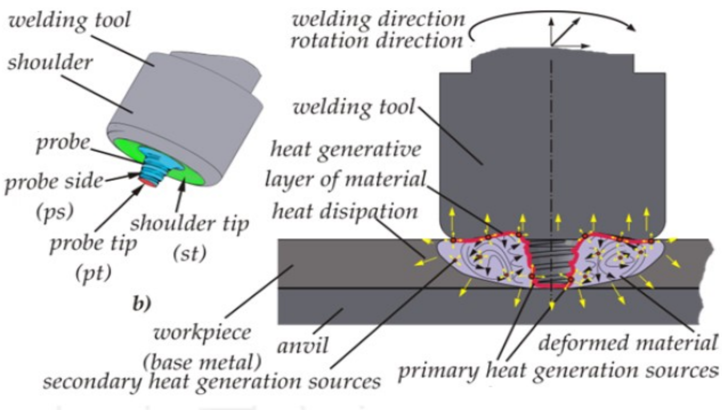

Fig. 1. Heat generation in FSW [11]

where the heat indexed with *fr* represents frictional heat, heat indexed with *def* represents deformation heat, δ_{pt}, δ_{ps}, δ_{st} are dimensionless contact state variable (extension of slip) at the pin tip, pin side and shoulder tip, respectively. According to Jauhari [12], $\delta_{pt}=0.1$, $\delta_{ps}= 0.2$ and $\delta_{st}= 0.1$. It should be noted that If δ is 1, full sticking condition is applied and all the heat is generated by plastics deformation. When $\delta = 0$, heat is generated only by friction.

The analytical estimation of heat generation is based on the following assumptions

i. Uniform contact shear stress $\tau_{contact}$ is considered.
ii. Weld cycle excludes plunging; first, second dwell, and retract cycles.
iii. Tool inclination angle was not considered.
iv. No heat flows into the workpiece if the local temperature reaches the material melting temperature.
v. The axial pressure is evenly distributed along z-axis
vi. Due to friction and deformation interface conditions, the frictional and deformation shear stresses are considered.
vii. The thread on the pin side of the welding tool was neglected

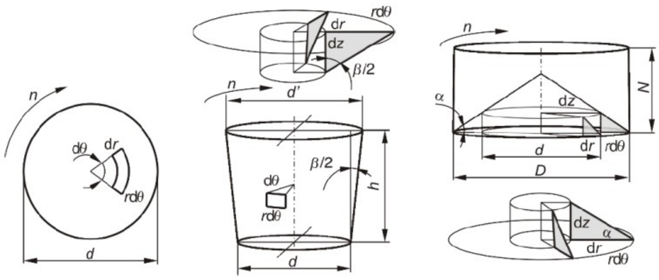

(a) (b) (c)

Fig. 2. Active surfaces in FSW: (a) pin tip, (b) pin side, (c) shoulder tip

The general expression for an infinitesimal amount of heat generation at each of the different zones of the tool/workpiece interface is given by

$$dQ = \omega r dF \tag{4}$$

where dQ is the heat generated per unit time, dF is the force acting on the surface at a distance r from the tool centerline and ω is the angular velocity of the tool.

$$dF = \tau_{contact} dA \tag{5}$$

where $\tau_{contact}$ is the contact shear stress and $dA = rdrd\theta$ is the area of the infinitesimal segment on the surface. The frictional and deformation amount of heat with respect to the contact shear stress is given by

$$\tau_{cont} = \begin{cases} \mu p & \textit{for frictional heat generation} \text{ (Coulumb's friction law)} \\ \tau_{yield} & \textit{for deformational heat generation} \end{cases} \tag{6}$$

where μ is the frictional coefficients, p is the contact pressure, τ_{yield} is the yield strength of the workpiece. Following Arora *et al.* [13], frictional coefficients can be calculated as

$$\mu = \mu_o exp\left(-\delta_{slip} \frac{\omega}{\omega_o} \frac{R_p}{R_s}\right) \tag{7}$$

Where μ_o is the static friction coefficient and it is taken as 0.45 [14, 15]. δ_{slip} is the slipping factor, ω is the rotating speed and the reference rotation speed ω_o is taken as 400 rpm. R_p and R_s are the radii of the tool pin and the shoulder, respectively. Where η_{fd} represents the fraction of the mechanical energy that is converted to frictional heat and deformational heat. Which could be as high as 0.99 based on the assumptions of previous work. The boundary value of the yield shear stress from the von Misses yield criterion in uniaxial tension and pure shear is given by

$$\tau_{yield} = \frac{\sigma_{yield}(T,\varepsilon)}{\sqrt{3}} \tag{8}$$

The yield strength of the workpiece's material, $\sigma_{yield}(T,\varepsilon)$ is highly dependent on temperature, T and strain rate, ε. The analysis of the tangential stresses within FSW requires the full temperature and strain history in the workpiece in a wide zone around the welding tool. Sheppard and Wright [16] elastic-plastic model may be used to evaluate the temperature-strain dependent yield strength of the workpiece's material, $\sigma_{yield}(T,\varepsilon)$.

$$\sigma_{yield}(T,\varepsilon) = \frac{1}{\alpha} sinh^{-1}\left[\left(\frac{Z(\varepsilon,\mathrm{T})}{A}\right)^{\frac{1}{n}}\right] \tag{9}$$

Where *A, α,* and *n* are material constants and Z(ε,T) is the Zener-Hollomon parameter that represents the temperature-compensated effective strain rate by

$$Z(\varepsilon,T) = \dot{\varepsilon} e\,\mathrm{xp}\left(\frac{Q}{RT}\right) \tag{10}$$

Where $\dot{\varepsilon}, Q, R,$ and T are strain rate, activation energy, universal gas constant and absolute temperature, respectively. While Sheppard and Jackson [17] developed the elastic-plastic model for yield strength of the workpiece's material as

$$\sigma_{yield}(T,\varepsilon) \approx \frac{1}{\alpha} In\left\{\left(\frac{Z(T,\varepsilon)}{A}\right)^{\frac{1}{n}} + \left[1+\left(\frac{Z(T,\varepsilon)}{A}\right)^{\frac{2}{n}}\right]^{\frac{1}{2}}\right\} \tag{11}$$

It was stated that the lack of the detailed material constitutive information and other thermal and physical properties at conditions such as very high strain rates and elevated temperatures seems to be the limiting factor while modeling the FSW process [18]. Consequently, Colegrove and Sherchiff [19] and Wang *et al.,* [20] pointed out that Sheppard and Jackson's elastic-plastic model is not applicable at the melting of the material. Although, Su *et al.* [21] modified the Sheppard and Jackson's elastic-plastic model as

$$\sigma_{yield}(T,\varepsilon) = \sigma_o + \left\{\frac{1}{\alpha}\left(1-\sqrt{\frac{T-273}{T-273}}\right) In\left\{\left(\frac{Z(T,\varepsilon)}{A}\right)^{\frac{1}{n}} + \left[1+\left(\frac{Z(T,\varepsilon)}{A}\right)^{\frac{2}{n}}\right]^{\frac{1}{2}}\right\}\right\} \tag{12}$$

In this work, we adopted a developed generic model [22]

$$\sigma_{yield}(T,\varepsilon) = \sigma_o + \left\{\frac{1}{\alpha}\left(1-\sqrt[p]{\frac{T-T_{room}}{T-T_{room}}}\right) In\left\{\left[\frac{\dot{\varepsilon}}{A} e\,\mathrm{xp}\left(\frac{Q}{RT}\right)\right]^{\frac{1}{n}} + \left[1+\left[\frac{\dot{\varepsilon}}{A} e\,\mathrm{xp}\left(\frac{Q}{RT}\right)\right]^{\frac{2}{n}}\right]^{\frac{1}{2}}\right\}\right\} \tag{13}$$

Where T_{room} is the room temperature and p is the model constant which ranges from $1.8 \le p \le 2.2$, depending on the material. σ_o is the yield stress beyond the melting point of the material. Alternatively, we have [22]

$$\sigma_{yield}(T,\varepsilon) = \sigma_o + \frac{1}{\alpha}\left\{\left(1-\sqrt[p]{\frac{T-T_{room}}{T-T_{room}}}\right)\sum_{p=1}^{\infty}(-1)^{p+1}\left(\frac{\dot{\varepsilon}}{A} e\,\mathrm{xp}\left(\frac{Q}{RT}\right)\right)^{2p-1} \frac{\prod_{p=1}^{\infty}(2p-1)}{\prod_{p=1}^{\infty}2p(2p+1)}\right\} \quad for \quad \left|\left(\frac{\dot{\varepsilon}}{A} e\,\mathrm{xp}\left(\frac{Q}{RT}\right)\right)\right| < 1 \tag{14}$$

On expanding Eq. (14), we have

$$\sigma_{yield}(T,\varepsilon) = \sigma_o + \frac{1}{\alpha}\left(1-\sqrt[p]{\frac{T-T_{room}}{T-T_{room}}}\right)\left\{\begin{array}{l}\left(\frac{\dot{\varepsilon}}{A} e\,\mathrm{xp}\left(\frac{Q}{RT}\right)\right)^{\frac{1}{n}} - \frac{1}{6}\left(\frac{\dot{\varepsilon}}{A} e\,\mathrm{xp}\left(\frac{Q}{RT}\right)\right)^{\frac{3}{n}} + \frac{3}{40}\left(\frac{\dot{\varepsilon}}{A} e\,\mathrm{xp}\left(\frac{Q}{RT}\right)\right)^{\frac{5}{n}} \\ -\frac{5}{112}\left(\frac{\dot{\varepsilon}}{A} e\,\mathrm{xp}\left(\frac{Q}{RT}\right)\right)^{\frac{7}{n}} + \frac{35}{1152}\left(\frac{\dot{\varepsilon}}{A} e\,\mathrm{xp}\left(\frac{Q}{RT}\right)\right)^{\frac{9}{n}}\end{array}\right\} \tag{15}$$

Another generic model developed by the author [22] is

$$\sigma_{yield}(T,\varepsilon)=\sigma_o+\frac{1}{\alpha}\left\{\frac{1}{n}In\left(\left(\frac{2\dot{\varepsilon}}{A}e\,\mathrm{xp}\left(\frac{Q}{RT}\right)\right)\right)+\sum_{m=1}^{\infty}(-1)^{m+1}\frac{(2m)!\left(\left(\frac{\dot{\varepsilon}}{A}e\,\mathrm{xp}\left(\frac{Q}{RT}\right)\right)\right)^{-2m}}{2^m(m!)^2 2m}\right\},\quad \left|\left(\frac{\dot{\varepsilon}}{A}e\,\mathrm{xp}\left(\frac{Q}{RT}\right)\right)\right|>1 \tag{16}$$

Which when expanded, we have

$$\sigma_{yield}(T,\varepsilon)=\sigma_o+\frac{1}{\alpha}\left(1-\sqrt[p]{\frac{T-T_{room}}{T-T_{room}}}\right)\left\{\begin{array}{l}\frac{1}{n}In\left(\frac{2\dot{\varepsilon}}{A}e\,\mathrm{xp}\left(\frac{Q}{RT}\right)\right)+\frac{1}{4}\left(\frac{\dot{\varepsilon}}{A}e\,\mathrm{xp}\left(\frac{Q}{RT}\right)\right)^{\frac{-2}{n}}\\ -\frac{3}{32}\left(\frac{\dot{\varepsilon}}{A}e\,\mathrm{xp}\left(\frac{Q}{RT}\right)\right)^{\frac{-4}{n}}+\frac{5}{96}\left(\frac{\dot{\varepsilon}}{A}e\,\mathrm{xp}\left(\frac{Q}{RT}\right)\right)^{\frac{-6}{n}}\\ -\frac{35}{1024}\left(\frac{\dot{\varepsilon}}{A}e\,\mathrm{xp}\left(\frac{Q}{RT}\right)\right)^{\frac{-8}{n}}+\frac{63}{2560}\left(\frac{\dot{\varepsilon}}{A}e\,\mathrm{xp}\left(\frac{Q}{RT}\right)\right)^{\frac{-10}{n}}\end{array}\right\} \tag{17}$$

However, in the analysis of heat generation in FSW, the influence of strain on the decrease of yield strength can be neglected and sufficient precision will still be maintained [23]. Neglecting strain effects on the yield strength is possible since the maximal temperatures of the material reach about 80% of the melting temperature when the strain has significant values due to near melting conditions in the material [13, 24]. Therefore, Eq. (16) becomes

$$\tau_{yield}=\frac{\sigma_{yield}(T)}{\sqrt{3}} \tag{18}$$

For Stainless steel, yield stress as developed in this work, we have

$$\sigma_{yield}(T)=\beta_o+\beta_1 T+\beta_2 T^2+\beta_3 T^3++\beta_4 T^4++\beta_5 T^5 \tag{19}$$

where

$$\beta_o=240,\ \beta_1=7.3583\times10^{-1},\ \ \beta_2=-7.1333\times10^{-2},\ \ \beta_3=2.163\times10^{-5},$$
$$\beta_4=-2.7292\times10^{-8}\ and\ \ \beta_5=1.1849\times10^{-8}$$

3. Development of Heat generation Models for different Pin and Shoulder Profiles

The pin geometry plays a vital role for material flow, temperature history, grain size, and mechanical properties in the FSW processes [8]. Therefore, heat generation models are developed for different pin profiles with flat and conical shoulder.

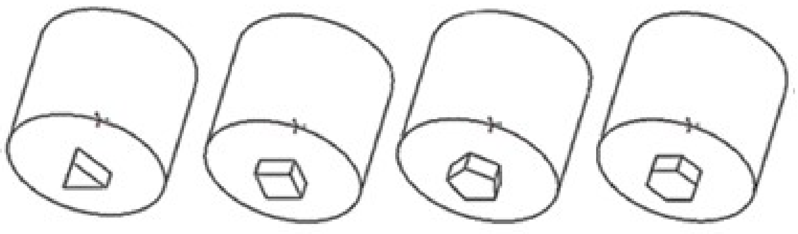

(a) (b) (c) (d)

(b) **Fig. 3.** Different profiles pin used in FSW Triangular pin (b) Square pin (c) Pentagonal pin (d) Hexagonal pin [8]

3.1 Triangle pin profile

The tool design for the triangular pin is presented in Fig. 3. As before, Q_{st} is the heat generated under the tool shoulder, Q_{ps} at the tool pin side and Q_{pt} at the tool pin tip. To derive the different quantities, the surface under examination is characterized by either being a vertical or horizontal surface.

For the shoulder tip frictional heat generation, we have

$$Q_{st}^{fr}=Q_{st}^{fr}=\int_0^{2\pi}\int_0^{R_s}u\,\mu prdrd\theta-6\int_0^{\frac{\pi}{3}}\int_0^{R_p}u\,\mu prdrd\theta \tag{20}$$

The factor '6' at the second term on the RHS of Eq. (20) denotes the six different regions that form the whole triangular surface.

$$Q_{st}^{fr}=\int_0^{2\pi}\int_0^{R_s}\mu pr\left(\omega r\pm v_w sin\theta\right)drd\theta-6\int_0^{\frac{\pi}{3}}\int_0^{R_p}\mu pr\left(\omega r\pm v_w sin\theta\right)drd\theta \tag{21}$$

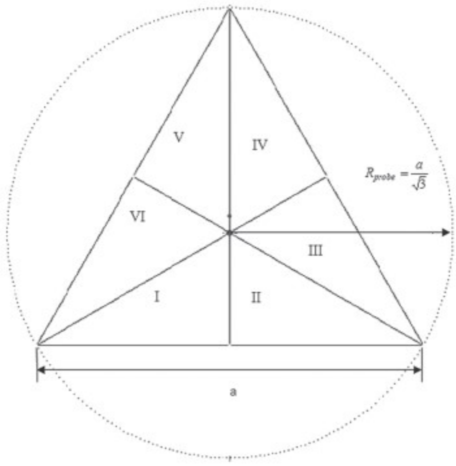

Fig. 4. Schematic of the triangular pin/probe [8].

Analytical prediction of the energy input into the weld material indicates that most comes from the angular motion. The translational force, in agreement with the analytical calculations, supplied very little power compared to input from angular rotation. This is consistent with dynamometer measurements. Therefore, after the integration as shown in Equ. (21) while neglecting the heat generated due to advancing and retracting, we arrived at

$$Q_{st}^{fr} = \frac{2}{3}\pi\omega\mu p\left(R_s^3 - R_p^3\right) \tag{22}$$

From the geometrical analysis of Fig. 4, $R_P = \frac{a}{\sqrt{3}}$

$$Q_{st}^{fr} = \frac{2}{3}\pi\mu p\left[\omega R_s^3 - \left(\frac{a^3\omega}{3\sqrt{3}} \pm \frac{a^2 v_w}{4}\right)\right] \tag{23}$$

If the heat generated due to advancing and retracting is neglected, then we have

$$Q_{st}^{fr} = \frac{2}{3}\pi\omega\mu p\left[R_s^3 - \frac{a^3}{3\sqrt{3}}\right] \tag{24}$$

Similarly, for the shoulder tip deformational heat generation,

$$Q_{st}^{def} = \frac{2}{3}\pi\omega\tau_{yield}\left(R_s^3 - \frac{a^3}{3\sqrt{3}}\right) \tag{25}$$

The total heat generation at the shoulder tip is

$$Q_{st} = \frac{2}{3}\pi\omega\mu p\left(R_s^3 - \frac{a^3}{3\sqrt{3}}\right)(1-\delta_{st}) + \frac{2}{3}\pi\omega\tau_{yield}\delta_{st}\left(R_s^3 - \frac{a^3}{3\sqrt{3}}\right) \tag{26}$$

Considering the fraction of the mechanical energy that is converted to frictional heat and deformational heat

$$Q_{st\eta} = \frac{2}{3}\pi\omega\eta_{fd}\left[\mu p\left(R_s^3 - \frac{a^3}{3\sqrt{3}}\right)(1-\delta_{st}) + \tau_{yield}\delta_{st}\left(R_s^3 - \frac{a^3}{3\sqrt{3}}\right)\right] \tag{27}$$

After rationalization, Equ. (27) gives

$$Q_{st\eta} = \frac{2}{3}\pi\omega\eta_{fd}\left[\mu p\left(R_s^3 - \frac{a^3\sqrt{3}}{9}\right)(1-\delta_{st}) + \tau_{yield}\delta_{st}\left(R_s^3 - \frac{a^3\sqrt{3}}{9}\right)\right] \tag{28}$$

If the shoulder is conical, then

$$Q_{st\eta} = \frac{2}{3}\pi\omega\eta_{fd}\left[\mu p\left(R_s^3 - \frac{a^3\sqrt{3}}{9}\right)(1-\delta_{st})\left(1+tan\,\alpha\right) + \tau_{yield}\delta_{st}\left(R_s^3 - \frac{a^3\sqrt{3}}{9}\right)\left(1+tan\,\alpha\right)\right] \tag{29}$$

For the pin tip frictional heat generation, the heat generation due to friction at the pin tip is

$$Q_{pt}^{fr} = 6\int_0^{\theta=\frac{\pi}{3}}\int_{R_p=0}^{R_p=\frac{a}{\sqrt{3}}} \omega r\,\mu p r dr d\theta \tag{30}$$

Again, the factor '6' at the second term on the RHS of Equ. (30) denotes the six different regions that form the whole triangular surface.

$$Q_{pt}^{fr} = 6\int_{0}^{\theta=\frac{\pi}{3}} \int_{R_p=0}^{R_p=\frac{a}{\sqrt{3}}} \mu pr\left(\omega r \pm v_w sin\theta\right) drd\theta \tag{31}$$

$$Q_{pt}^{fr} = 6\mu p\left[\omega\int_{0}^{\theta=\frac{\pi}{3}} \int_{R_p=0}^{R_p=\frac{a}{\sqrt{3}}} r^2 drd\theta \pm v_w \int_{0}^{\theta=\frac{\pi}{3}} \int_{R_p=0}^{R_p=\frac{a}{\sqrt{3}}} rsin\theta drd\theta\right] \tag{32}$$

After the above integration as shown in Equ. (32), we arrived at

$$Q_{pt}^{fr} = \frac{2}{3}\pi\omega\mu pa^2\left(\frac{a\sqrt{3}}{9} \pm \frac{v_w}{4\omega\pi}\right) \tag{33}$$

Similarly, for the pin tip deformational heat generation,

$$Q_{pt}^{def} = \frac{2}{3}\pi\omega\tau_{yield} a^2\left(\frac{a\sqrt{3}}{9} \pm \frac{v_w}{4\omega\pi}\right) \tag{34}$$

Therefore, the total heat generation at the pin tip is

$$Q_{pt} = \frac{2}{3}\pi\omega\mu pa^2\left(\frac{a\sqrt{3}}{9} \pm \frac{v_w}{4\omega\pi}\right)(1-\delta_{pt}) + \frac{2}{3}\pi\omega\tau_{yield} a^2\delta_{pt}\left(\frac{a\sqrt{3}}{9} \pm \frac{v_w}{4\omega\pi}\right) \tag{35}$$

Then

$$Q_{pt\eta} = \frac{2}{3}\pi\omega a^2\eta_{fd}\left[\mu p\left(\frac{a\sqrt{3}}{9} \pm \frac{v_w}{4\omega\pi}\right)(1-\delta_{pt}) + \tau_{yield}\delta_{pt}\left(\frac{a\sqrt{3}}{9} \pm \frac{v_w}{4\omega\pi}\right)\right] \tag{36}$$

If the heat generated due to advancing and retracting is neglected, then Eq. (36) becomes

$$Q_{pt\eta} = \frac{2}{3}\eta_{fd}\pi\omega a^3\left[\frac{\sqrt{3}}{9}\mu pa(1-\delta_{pt}) + \frac{\sqrt{3}}{9}\tau_{yield}\delta_{pt}\right] \tag{37}$$

For the pin side frictional heat generation, the heat generation due to friction at the pin side is

$$Q_{ps}^{fr} = 3\int_{R_p=0}^{R_p=a} \int_{L=0}^{L=L_p} \omega r\,\mu prdxdy \tag{38}$$

The factor '3' at the RHS of Equ. (38) denotes the three sides of the triangular pin. After substitution of the velocity,

$$Q_{ps}^{fr} = 3\int_{R_p=0}^{R_p=a} \int_{L=0}^{L=L_p} \left(\omega r \pm v_w sin\theta\right)\mu pdxdy \tag{39}$$

$$Q_{ps}^{fr} = \mu p\left[\omega\int_{R_p=0}^{R_p=a} \int_{L=0}^{L=L_p} R_p dR_p dy + v_w \int_{R_p=0}^{R_p=a} \int_{L=0}^{L=L_p} sin\theta drdy\right] \tag{40}$$

After the integration as shown in Equ. (40), we arrived at

$$Q_{ps}^{fr} = \frac{1}{2}\omega\mu pa^2 L_p + 3v_w\,\mu paL_p sin\theta \tag{41}$$

Similarly, for the pin side deformational heat generation,

$$Q_{ps}^{def} = \frac{1}{2}\omega\tau_{yield} a^2 L_p + 3v_w\,\tau_{yield} aL_p sin\theta \tag{42}$$

The total heat generation at the pin side is

$$Q_{ps} = \mu paL_p\left(\frac{1}{2}\omega a + 3v_w sin\theta\right)(1-\delta_{st}) + \tau_{yeild} aL_p\left(\frac{1}{2}\omega a + 3v_w sin\theta\right)\delta_{st} \tag{43}$$

and

$$Q_{ps\eta} == \eta_{fd} aL_p\left[\mu p\left(\frac{1}{2}\omega a + 3v_w sin\theta\right)(1-\delta_{ps}) + \tau_{yeild}\left(\frac{1}{2}\omega a + 3v_w sin\theta\right)\delta_{ps}\right] \tag{44}$$

If the heat generated due to advancing and retracting is neglected, then we have

$$Q_{ps\eta} == \frac{1}{2}\eta_{fd}\omega a^2 L_p\left[\mu p(1-\delta_{st}) + \tau_{yeild}\delta_{st}\right] \tag{45}$$

The total heat generation for the triangular profile pin with flat shoulder is the summation of Equs. (24), (37) and (45):

$$Q_{total} = \eta_{fd}\,\omega \begin{bmatrix} \frac{2}{3}\pi\left[\mu p\left(R_s^3 - \frac{a^3\sqrt{3}}{9}\right)(1-\delta_{st}) + \tau_{yield}\delta_{st}\left(R_s^3 - \frac{a^3\sqrt{3}}{9}\right)\right] \\ +\frac{2}{3}\pi a^3\left[\frac{\sqrt{3}}{9}\mu p(1-\delta_{pt}) + \frac{\sqrt{3}}{9}\tau_{yield}\delta_{pt}\right] \\ +\frac{1}{2}a^2 L_p\left[\mu p(1-\delta_{ps}) + \tau_{yeild}\delta_{ps}\right] \end{bmatrix} \tag{46}$$

Fraction of heat generation at the shoulder

$$f_s = \frac{Q_{st}}{Q_{total}} = \frac{\frac{2}{3}\pi\left[\mu p\left(R_s^3 - \frac{a^3\sqrt{3}}{9}\right)(1-\delta_{st}) + \tau_{yield}\delta_{st}\left(R_s^3 - \frac{a^3\sqrt{3}}{9}\right)\right]}{\begin{bmatrix} \frac{2}{3}\pi\left[\mu p\left(R_s^3 - \frac{a^3\sqrt{3}}{9}\right)(1-\delta_{st}) + \tau_{yield}\delta_{st}\left(R_s^3 - \frac{a^3\sqrt{3}}{9}\right)\right] \\ +\frac{2}{3}\pi a^3\left[\frac{\sqrt{3}}{9}\mu p(1-\delta_{pt}) + \frac{\sqrt{3}}{9}\tau_{yield}\delta_{pt}\right] \\ +\frac{1}{2}a^2 L_p\left[\mu p(1-\delta_{ps}) + \tau_{yeild}\delta_{ps}\right] \end{bmatrix}} \tag{47}$$

Fraction of heat generation at the pin

$$f_p = \frac{Q_p}{Q_{total}} = \frac{\frac{2}{3}\pi a^2\left[\frac{\sqrt{3}}{9}\mu pa(1-\delta_{pt}) + \frac{\sqrt{3}}{9}\tau_{yield}\delta_{pt}\right] + \frac{1}{2}a^2 L_p\left[\mu p(1-\delta_{ps}) + \tau_{yeild}\delta_{ps}\right]}{\begin{bmatrix} \frac{2}{3}\pi\left[\mu p\left(R_s^3 - \frac{a^3\sqrt{3}}{9}\right)(1-\delta_{st}) + \tau_{yield}\delta_{st}\left(R_s^3 - \frac{a^3\sqrt{3}}{9}\right)\right] \\ +\frac{2}{3}\pi a^2\left[\frac{\sqrt{3}}{9}\mu pa(1-\delta_{pt}) + \frac{\sqrt{3}}{9}\tau_{yield}\delta_{pt}\right] \\ +\frac{1}{2}a^2 L_p\left[\mu p(1-\delta_{ps}) + \tau_{yeild}\delta_{ps}\right] \end{bmatrix}} \tag{48}$$

The energy per unit length of the weld for the flat shoulder tool is

$$Q'_{Energy} = \frac{\omega\eta_{fd}}{vR_s^2}\begin{bmatrix} \frac{2}{3}\left[\mu F\left(R_s^3 - \frac{a^3\sqrt{3}}{9}\right)(1-\delta_{st}) + \tau_{yield}A_s\delta_{st}\left(R_s^3 - \frac{a^3\sqrt{3}}{9}\right)\right] \\ +\frac{2}{3}a^2\left[\frac{\sqrt{3}}{9}\mu Fa(1-\delta_{pt}) + \frac{\sqrt{3}}{9}\tau_{yield}A_s\delta_{pt}\right] + \frac{1}{2\pi}a^2 L_p\left[\mu F(1-\delta_{ps}) + \tau_{yeild}A_s\delta_{ps}\right] \end{bmatrix} \tag{49}$$

While the total heat generation for the triangular profile pin with conical shoulder is given as

$$Q_{total} = \eta_{fd}\,\omega\begin{bmatrix} \frac{2}{3}\pi\left[\mu p\left(R_s^3 - \frac{a^3\sqrt{3}}{9}\right)(1-\delta_{st})(1+tan\,\alpha) + \tau_{yield}\delta_{st}\left(R_s^3 - \frac{a^3\sqrt{3}}{9}\right)(1+tan\,\alpha)\right] \\ +\frac{2}{3}\pi a^2\left[\frac{\sqrt{3}}{9}\mu pa(1-\delta_{pt}) + \frac{\sqrt{3}}{9}\tau_{yield}\delta_{pt}\right] + \frac{1}{2}a^2 L_p\left[\mu p(1-\delta_{ps}) + \tau_{yeild}\delta_{ps}\right] \end{bmatrix} \tag{50}$$

Fraction of heat generation at the shoulder

$$f_s = \frac{Q_{st}}{Q_{total}} = \frac{\frac{2}{3}\pi\left[\mu p\left(R_s^3 - \frac{a^3\sqrt{3}}{9}\right)(1-\delta_{st})(1+tan\,\alpha) + \tau_{yield}\delta_{st}\left(R_s^3 - \frac{a^3\sqrt{3}}{9}\right)(1+tan\,\alpha)\right]}{\begin{bmatrix} \frac{2}{3}\pi\left[\mu p\left(R_s^3 - \frac{a^3\sqrt{3}}{9}\right)(1-\delta_{st})(1+tan\,\alpha) + \tau_{yield}\delta_{st}\left(R_s^3 - \frac{a^3\sqrt{3}}{9}\right)(1+tan\,\alpha)\right] \\ +\frac{2}{3}\pi a^2\left[\frac{\sqrt{3}}{9}\mu pa(1-\delta_{pt}) + \frac{\sqrt{3}}{9}\tau_{yield}\delta_{pt}\right] + \frac{1}{2}a^2 L_p\left[\mu p(1-\delta_{ps}) + \tau_{yield}\delta_{ps}\right] \end{bmatrix}} \tag{51}$$

Fraction of heat generation at the pin

$$f_p = \frac{Q_p}{Q_{total}} = \frac{\frac{2}{3}\pi a^2\left[\frac{\sqrt{3}}{9}\mu pa(1-\delta_{pt}) + \frac{\sqrt{3}}{9}\tau_{yield}\delta_{pt}\right] + \frac{1}{2}a^2 L_p\left[\mu p(1-\delta_{ps}) + \tau_{yeild}\delta_{ps}\right]}{\left[\begin{array}{l}\frac{2}{3}\pi\left[\mu p\left(R_s^3 - \frac{a^3\sqrt{3}}{9}\right)(1-\delta_{st})(1+tan\alpha) + \tau_{yield}\delta_{st}\left(R_s^3 - \frac{a^3\sqrt{3}}{9}\right)(1+tan\alpha)\right] \\ +\frac{2}{3}\pi a^2\left[\frac{\sqrt{3}}{9}\mu pa(1-\delta_{pt}) + \frac{\sqrt{3}}{9}\tau_{yield}\delta_{pt}\right] + \frac{1}{2}a^2 L_p\left[\mu p(1-\delta_{ps}) + \tau_{yeild}\delta_{ps}\right]\end{array}\right]} \tag{52}$$

The energy per unit length of the weld for the conical shoulder tool is

$$Q'_{Energy} = \frac{\omega\eta_{fd}}{vR_s^2}\left[\begin{array}{l}\frac{2}{3}\left[\mu F\left(R_s^3 - \frac{a^3\sqrt{3}}{9}\right)(1-\delta_{st})(1+tan\alpha) + \tau_{yield}A_s\delta_{st}\left(R_s^3 - \frac{a^3\sqrt{3}}{9}\right)(1+tan\alpha)\right] \\ +\frac{2}{3}a^2\left[\frac{\sqrt{3}}{9}\mu Fa(1-\delta_{pt}) + \frac{\sqrt{3}}{9}\tau_{yield}A_s\delta_{pt}\right] + \frac{1}{2\pi}a^2 L_p\left[\mu F(1-\delta_{ps}) + \tau_{yeild}A_s\delta_{ps}\right]\end{array}\right] \tag{53}$$

3.2 Square pin profile

The tool design for the square pin is presented in Fig. 5. Again, to derive the different quantities, the surface under examination is characterized by either being a vertical or horizontal surface.

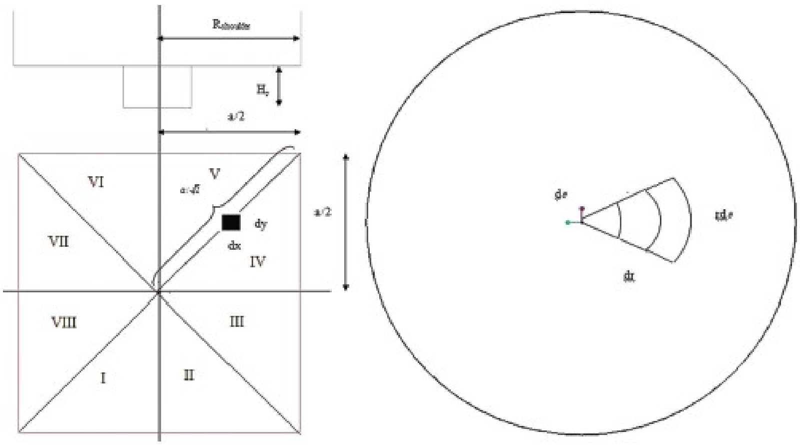

Fig. 5. Schematic of the surface orientations and infinitesimal segment areas square pin [8].

As before, for the shoulder tip frictional heat generation, we have

$$Q_{st}^{fr} = \int_0^{2\pi}\int_0^{R_s} u\,\mu prdrd\theta - 8\int_0^{\frac{\pi}{4}}\int_0^{R_p} u\,\mu prdrd\theta \tag{54}$$

Again, the factor ‘8’ at the second term on the RHS of Equ. (54) denotes the six different regions that form the whole square surface.

$$Q_{st}^{fr} = \int_0^{2\pi}\int_0^{R_s} \mu p\left(\omega r \pm v_w sin\theta\right)r\;\;drd\theta - 8\int_0^{\frac{\pi}{4}}\int_0^{R_p} \mu pr\left(\omega r \pm v_w sin\theta\right)drd\theta \tag{55}$$

Carrying out the integration of Equ. (55) while neglecting the heat generated due to advancing and retracting, gives

$$Q_{st}^{fr} = \frac{2}{3}\pi\omega\mu p\left(R_s^3 - R_p^3\right) \tag{56}$$

From the geometrical analysis of Fig. 5, $R_P = \frac{a}{\sqrt{2}}$

$$Q_{st}^{fr} = \frac{2}{3}\pi\omega\mu p\left(R_s^3 - \frac{a^3}{2\sqrt{2}}\right) \tag{57}$$

Similarly, for the shoulder tip deformational heat generation,

$$Q_{st}^{def} = \frac{2}{3}\pi\omega\tau_{yield}\left(R_s^3 - \frac{a^3}{2\sqrt{2}}\right) \tag{58}$$

The total heat generation at the shoulder tip is

$$Q_{st} = \frac{2}{3}\pi\omega\mu p\left(R_s^3 - \frac{a^3}{2\sqrt{2}}\right)(1-\delta_{st}) + \frac{2}{3}\pi\omega\tau_{yield}\left(R_s^3 - \frac{a^3}{2\sqrt{2}}\right) \tag{59}$$

while

$$Q_{st\eta} = \frac{2}{3}\pi\omega\eta_{fd}\left[\mu p\left(R_s^3 - \frac{a^3}{2\sqrt{2}}\right)(1-\delta_{st}) + \tau_{yield}\delta_{st}\left(R_s^3 - \frac{a^3}{2\sqrt{2}}\right)\right] \tag{60}$$

After rationalization, Equ. (60) gives

$$Q_{st\eta} = \frac{2}{3}\pi\omega\eta_{fd}\left[\mu p\left(R_s^3 - \frac{a^3\sqrt{2}}{4}\right)(1-\delta_{st}) + \tau_{yield}\delta_{st}\left(R_s^3 - \frac{a^3\sqrt{2}}{4}\right)\right] \tag{61}$$

If the shoulder is conical, then

$$Q_{st\eta} = \frac{2}{3}\pi\omega\eta_{fd}\left[\mu p\left(R_s^3 - \frac{a^3\sqrt{2}}{4}\right)(1-\delta_{st})\left(1+tan\,\alpha\right) + \tau_{yield}\delta_{st}\left(R_s^3 - \frac{a^3\sqrt{2}}{4}\right)\left(1+tan\,\alpha\right)\right] \tag{62}$$

For the pin tip frictional heat generation, we have

$$Q_{pt}^{fr} = 8\int_0^{\frac{\pi}{4}}\int_0^{R_p}\mu pr\left(\omega r \pm v_w sin\theta\right)drd\theta \tag{63}$$

The expansion of Eq.(63) gives

$$Q_{pt}^{fr} = 8\mu p\left[\omega\int_0^{\theta=\frac{\pi}{4}}\int_{R_p=0}^{R_p=\frac{a}{\sqrt{2}}} r^2 drd\theta \pm v_w\int_0^{\theta=\frac{\pi}{2}}\int_{R_p=0}^{R_p=\frac{a}{\sqrt{2}}} rsin\theta drd\theta\right] \tag{64}$$

After the above integration as shown in Equ. (64), while neglecting the heat generated due to advancing and retracting, we arrived at

$$Q_{st}^{fr} = \frac{2}{3}\pi\omega\mu pR_p \tag{65}$$

But from the geometrical analysis of Fig. 5, $R_P = \frac{a}{\sqrt{2}}$

$$Q_{st}^{fr} = \frac{2}{3}\pi\omega\mu p\frac{a^3}{2\sqrt{2}} \tag{66}$$

Similarly, for the pin tip deformational heat generation

$$Q_{st}^{def} = \frac{2}{3}\pi\omega\tau_{yield}\frac{a^3}{2\sqrt{2}} \tag{67}$$

The total heat generation at the pin tip is

$$Q_{st} = \frac{2}{3}\pi\omega\mu p\frac{a^3}{2\sqrt{2}}(1-\delta_{st}) + \frac{2}{3}\pi\omega\tau_{yield}\frac{a^3}{2\sqrt{2}} \tag{68}$$

and

$$Q_{st\eta} = \frac{2}{3}\pi\omega\eta_{fd}\left[\mu p\frac{a^3}{2\sqrt{2}}(1-\delta_{pt}) + \tau_{yield}\delta_{pt}\frac{a^3}{2\sqrt{2}}\right] \tag{69}$$

After rationalization, Equ. (69) gives

$$Q_{st\eta} = \frac{2}{3}\pi\omega\eta_{fd}\left[\mu p\frac{a^3\sqrt{2}}{4}(1-\delta_{pt}) + \tau_{yield}\delta_{pt}\frac{a^3\sqrt{2}}{4}\right] \tag{70}$$

For the pin side frictional heat generation, we have

$$Q_{ps}^{fr} = 4\int_{R_p=0}^{R_p=a}\int_{L=0}^{L=L_p}\omega r\,\mu prdxdy \tag{71}$$

The factor ‘8’ at the RHS of Equ. (71) denotes the three sides of the square pin.

$$Q_{ps}^{fr} = 4\int_{R_p=0}^{R_p=a}\int_{L=0}^{L=L_p}\omega r\,\mu prdxdy \tag{72}$$

Substituting the velocity,

$$Q_{ps}^{fr} = 4\int_{R_p=0}^{R_p=a} \int_{L=0}^{L=L_p} \left(\omega r \pm v_w sin\theta\right)\mu p dx dy \tag{73}$$

which gives

$$Q_{ps}^{fr} = \frac{1}{2}\mu p\left[\omega\int_{R_p=0}^{R_p=a} \int_{L=0}^{L=L_p} rdrdy + v_w \int_{R_p=0}^{R_p=a} \int_{L=0}^{L=L_p} sin\theta drdy\right] \tag{74}$$

Integration of Equ. (74) neglecting the heat generated due to advancing and retracting, gives

$$Q_{ps}^{fr} = \frac{1}{4}\omega\mu p a^2 L_p \tag{75}$$

Similarly, for the pin side deformational heat generation,

$$Q_{ps}^{def} = \frac{1}{4}\omega\tau_{yield} a^2 L_p \tag{76}$$

The total heat generation at the pin side is

$$Q_{ps} = \frac{1}{4}\omega a^2 \mu p L_p (1-\delta_{ps}) + \frac{1}{4}\omega a^2 \tau_{yeild} L_p \delta_{ps} \tag{77}$$

Then

$$Q_{ps\eta} = \frac{1}{4}\eta_{fd}\,\omega a^2 L_p\left[\mu p(1-\delta_{ps}) + \tau_{yeild}\delta_{ps}\right] \tag{78}$$

Therefore, the total heat generation for the square profile pin with flat shoulder is given as

$$Q_{total} = \eta_{fd}\,\omega\left[\begin{array}{l} \frac{2}{3}\pi\left[\mu p\left(R_s^3 - \frac{a^3\sqrt{2}}{4}\right)(1-\delta_{st}) + \tau_{yield}\delta_{st}\left(R_s^3 - \frac{a^3\sqrt{2}}{4}\right)\right] \\ +\frac{2}{3}\pi\left[\mu p\frac{a^3\sqrt{2}}{4}(1-\delta_{pt}) + \tau_{yield}\delta_{pt}\frac{a^3\sqrt{2}}{4}\right] \\ +\frac{1}{4}a^2 L_p\left[\mu p(1-\delta_{ps}) + \tau_{yeild}\delta_{ps}\right] \end{array}\right] \tag{79}$$

Fraction of heat generation at the shoulder

$$f_s = \frac{Q_{st}}{Q_{total}} = \frac{\frac{2}{3}\pi\left[\mu p\left(R_s^3 - \frac{a^3\sqrt{2}}{4}\right)(1-\delta_{st}) + \tau_{yield}\delta_{st}\left(R_s^3 - \frac{a^3\sqrt{2}}{4}\right)\right]}{\left[\begin{array}{l} \frac{2}{3}\pi\left[\mu p\left(R_s^3 - \frac{a^3\sqrt{2}}{4}\right)(1-\delta_{st}) + \tau_{yield}\delta_{st}\left(R_s^3 - \frac{a^3\sqrt{2}}{4}\right)\right] \\ +\frac{2}{3}\pi\left[\mu p\frac{a^3\sqrt{2}}{4}(1-\delta_{pt}) + \tau_{yield}\delta_{pt}\frac{a^3\sqrt{2}}{4}\right] \\ +\frac{1}{4}a^2 L_p\left[\mu p(1-\delta_{ps}) + \tau_{yeild}\delta_{ps}\right] \end{array}\right]} \tag{80}$$

Fraction of heat generation at the pin

$$f_p = \frac{Q_p}{Q_{total}} = \frac{\frac{2}{3}\pi\left[\mu p\frac{a^3\sqrt{2}}{4}(1-\delta_{pt}) + \tau_{yield}\delta_{pt}\frac{a^3\sqrt{2}}{4}\right] + \frac{1}{4}a^2 L_p\left[\mu p(1-\delta_{ps}) + \tau_{yeild}\delta_{ps}\right]}{\left[\begin{array}{l} \frac{2}{3}\pi\left[\mu p\left(R_s^3 - \frac{a^3\sqrt{2}}{4}\right)(1-\delta_{st}) + \tau_{yield}\delta_{st}\left(R_s^3 - \frac{a^3\sqrt{2}}{4}\right)\right] \\ +\frac{2}{3}\pi\left[\mu p\frac{a^3\sqrt{2}}{4}(1-\delta_{pt}) + \tau_{yield}\delta_{pt}\frac{a^3\sqrt{2}}{4}\right] \\ +\frac{1}{4}a^2 L_p\left[\mu p(1-\delta_{ps}) + \tau_{yeild}\delta_{ps}\right] \end{array}\right]} \tag{81}$$

The energy per unit length of the weld for the flat shoulder tool is

$$Q'_{Energy}=\frac{\omega\eta_{fd}}{vR_s^2}\begin{bmatrix}\frac{2}{3}\left[\mu F\left(R_s^3-\frac{a^3\sqrt{2}}{4}\right)(1-\delta_{st})+\tau_{yield}A_s\delta_{st}\left(R_s^3-\frac{a^3\sqrt{2}}{4}\right)\right]\\+\frac{2}{3}\left[\mu F\frac{a^3\sqrt{2}}{4}(1-\delta_{pt})+\tau_{yield}A_s\delta_{pt}\frac{a^3\sqrt{2}}{4}\right]\\+\frac{1}{4\pi}a^2L_p\left[\mu F(1-\delta_{ps})+\tau_{yeild}A_s\delta_{ps}\right]\end{bmatrix} \tag{82}$$

While the total heat generation for the square profile pin with conical shoulder is given as

$$Q_{total}=\eta_{fd}\omega\begin{bmatrix}\frac{2}{3}\pi\left[\mu p\left(R_s^3-\frac{a^3\sqrt{2}}{4}\right)(1-\delta_{st})(1+tan\alpha)+\tau_{yield}\delta_{st}\left(R_s^3-\frac{a^3\sqrt{2}}{4}\right)(1+tan\alpha)\right]\\+\frac{2}{3}\pi\left[\mu p\frac{a^3\sqrt{2}}{4}(1-\delta_{pt})+\tau_{yield}\delta_{pt}\frac{a^3\sqrt{2}}{4}\right]+\frac{1}{4}a^2L_p\left[\mu p(1-\delta_{ps})+\tau_{yeild}\delta_{ps}\right]\end{bmatrix} \tag{83}$$

Fraction of heat generation at the shoulder

$$f_s=\frac{Q_{st}}{Q_{total}}=\frac{\frac{2}{3}\pi\left[\mu p\left(R_s^3-\frac{a^3\sqrt{2}}{4}\right)(1-\delta_{st})(1+tan\alpha)+\tau_{yield}\delta_{st}\left(R_s^3-\frac{a^3\sqrt{2}}{4}\right)(1+tan\alpha)\right]}{\begin{bmatrix}\frac{2}{3}\pi\left[\mu p\left(R_s^3-\frac{a^3\sqrt{2}}{4}\right)(1-\delta_{st})(1+tan\alpha)+\tau_{yield}\delta_{st}\left(R_s^3-\frac{a^3\sqrt{2}}{4}\right)(1+tan\alpha)\right]\\+\frac{2}{3}\pi\left[\mu p\frac{a^3\sqrt{2}}{4}(1-\delta_{pt})+\tau_{yield}\delta_{pt}\frac{a^3\sqrt{2}}{4}\right]+\frac{1}{4}a^2L_p\left[\mu p(1-\delta_{ps})+\tau_{yeild}\delta_{ps}\right]\end{bmatrix}} \tag{84}$$

Fraction of heat generation at the pin

$$f_p=\frac{Q_p}{Q_{total}}=\frac{\frac{2}{3}\pi\left[\mu p\frac{a^3\sqrt{2}}{4}(1-\delta_{pt})+\tau_{yield}\delta_{pt}\frac{a^3\sqrt{2}}{4}\right]+\frac{1}{4}a^2L_p\left[\mu p(1-\delta_{ps})+\tau_{yeild}\delta_{ps}\right]}{\begin{bmatrix}\frac{2}{3}\pi\left[\mu p\left(R_s^3-\frac{a^3\sqrt{2}}{4}\right)(1-\delta_{st})(1+tan\alpha)+\tau_{yield}\delta_{st}\left(R_s^3-\frac{a^3\sqrt{2}}{4}\right)(1+tan\alpha)\right]\\+\frac{2}{3}\pi\left[\mu p\frac{a^3\sqrt{2}}{4}(1-\delta_{pt})+\tau_{yield}\delta_{pt}\frac{a^3\sqrt{2}}{4}\right]+\frac{1}{4}a^2L_p\left[\mu p(1-\delta_{ps})+\tau_{yeild}\delta_{ps}\right]\end{bmatrix}} \tag{85}$$

The energy per unit length of the weld for the conical shoulder tool is

$$Q'_{Energy}=\frac{\omega\eta_{fd}}{vR_s^2}\begin{bmatrix}\frac{2}{3}\pi\left[\mu p\left(R_s^3-\frac{a^3\sqrt{2}}{4}\right)(1-\delta_{st})(1+tan\alpha)+\tau_{yield}\delta_{st}\left(R_s^3-\frac{a^3\sqrt{2}}{4}\right)(1+tan\alpha)\right]\\+\frac{2}{3}\pi\left[\mu p\frac{a^3\sqrt{2}}{4}(1-\delta_{pt})+\tau_{yield}\delta_{pt}\frac{a^3\sqrt{2}}{4}\right]+\frac{1}{4\pi}a^2L_p\left[\mu p(1-\delta_{ps})+\tau_{yeild}\delta_{ps}\right]\end{bmatrix} \tag{86}$$

3.3 Pentagonal pin profile

The tool design for the pentagonal pin is presented in Fig. 6. Deriving the different quantities, the surface under examination is characterized by either being a vertical or horizontal surface. As before, for the shoulder tip frictional heat generation, we have

$$Q_{st}^{fr}=\int_0^{2\pi}\int_0^{R_s}u\,\mu prdrd\theta-10\int_0^{\frac{\pi}{5}}\int_0^{R_p}u\,\mu prdrd\theta \tag{87}$$

Again, the factor ‘10’ at the second term on the RHS of Equ. (87) denotes the six different regions that form the whole pentagonal surface.

$$Q_{st}^{fr}=\int_0^{2\pi}\int_0^{R_s}\mu p\left(\omega r\pm v_w sin\theta\right)r\ \ drd\theta-10\int_0^{\frac{\pi}{5}}\int_0^{R_p}\mu pr\left(\omega r\pm v_w sin\theta\right)drd\theta \tag{88}$$

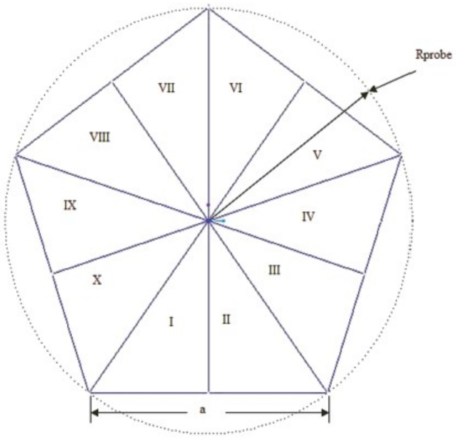

Fig. 6. Schematic of the pentagonal pin/probe [8].

Carrying out the Integration in Equ. (88) while neglecting the heat generated due to advancing and retracting, gives

$$Q_{st}^{fr} = \frac{2}{3}\pi\omega\mu p\left(R_s^3 - R_p^3\right) \tag{89}$$

From the geometrical analysis of Fig. 6, $R_P = 0.8506a$

$$Q_{st}^{fr} = \frac{2}{3}\pi\omega\mu p\left(R_s^3 - 0.6155a^3\right) \tag{90}$$

Similarly, for the shoulder tip deformational heat generation,

$$Q_{st}^{def} = \frac{2}{3}\pi\omega\tau_{yield}\left(R_s^3 - 0.6155a^3\right) \tag{91}$$

The total heat generation at the shoulder tip is

$$Q_{st} = \frac{2}{3}\pi\omega\mu p\left(R_s^3 - 0.6155a^3\right)(1-\delta_{st}) + \frac{2}{3}\pi\omega\tau_{yield}\left(R_s^3 - 0.6155a^3\right) \tag{92}$$

Then

$$Q_{st\eta} = \frac{2}{3}\pi\omega\eta_{fd}\left[\mu p\left(R_s^3 - 0.6155a^3\right)(1-\delta_{st}) + \tau_{yield}\left(R_s^3 - 0.6155a^3\right)\right] \tag{93}$$

If the shoulder is conical, then

$$Q_{st\eta} = \frac{2}{3}\pi\omega\eta_{fd}\begin{bmatrix}\mu p\left(R_s^3 - 0.6155a^3\right)(1-\delta_{st})\left(1+tan\alpha\right) \\ +\tau_{yield}\left(R_s^3 - 0.6155a^3\right)\left(1+tan\alpha\right)\end{bmatrix} \tag{94}$$

For the pin tip frictional heat generation, we have

$$Q_{pt}^{fr} = 10\int_0^{\frac{\pi}{5}}\int_0^{R_p}\mu pr\left(\omega r \pm v_w sin\theta\right)drd\theta \tag{95}$$

Expansion of Eq.(95) gives

$$Q_{pt}^{fr} = 10\mu p\left[\omega\int_0^{\theta=\frac{\pi}{5}}\int_{R_p=0}^{R_p} r^2 drd\theta \pm v_w\int_0^{\theta=\frac{\pi}{5}}\int_{R_p=0}^{R_p} rsin\theta drd\theta\right] \tag{96}$$

After the integration as shown in Equ. (96) while neglecting the heat generated due to advancing and retracting, we obtained from the geometrical analysis of Fig. 6, $R_P = 0.8506a$

$$Q_{st}^{fr} = \frac{2}{3}\pi\omega\mu p(0.6155a^3) \tag{97}$$

Similarly, for the pin tip deformational heat generation,

$$Q_{st}^{def} = \frac{2}{3}\pi\omega\tau_{yield}(0.6155a^3) \tag{98}$$

The total heat generation at the pin tip is

$$Q_{st} = \frac{2}{3}\pi\omega\mu p(0.6155a^3)(1-\delta_{st}) + \frac{2}{3}\pi\omega\tau_{yield}(0.6155a^3)\delta_{st} \tag{99}$$

while

$$Q_{st\eta} = \frac{2}{3}\pi\omega\eta_{fd}\left[\mu p(0.6155a^3)(1-\delta_{pt}) + \tau_{yield}\delta_{pt}(0.6155a^3)\right] \tag{100}$$

For the pin side frictional heat generation, we have

$$Q_{ps}^{fr} = 5\int_{R_p=0}^{R_p=a}\int_{L=0}^{L=L_p} \omega r\,\mu prdxdy \tag{101}$$

The factor '5' at the RHS of Equ. (101) denotes the three sides of the pentagonal pin.

$$Q_{ps}^{fr} = 5\int_{R_p=0}^{R_p=a}\int_{L=0}^{L=L_p} \omega r\,\mu prdxdy \tag{102}$$

Considering advancing and retracting,

$$Q_{ps}^{fr} = 5\int_{R_p=0}^{R_p=a}\int_{L=0}^{L=L_p} \left(\omega r \pm v_w \sin\theta\right)\mu pdxdy \tag{103}$$

As done previously,

$$Q_{ps}^{fr} = 0.36176\mu p\left[\omega\int_{R_p=0}^{R_p=a}\int_{L=0}^{L=L_p} rdrdy + v_w\int_{R_p=0}^{R_p=a}\int_{L=0}^{L=L_p} \sin\theta drdy\right] \tag{104}$$

On carrying out the integration as shown in the above Eq. (104), while neglecting the heat generated due to advancing and retracting, we arrived at

$$Q_{ps}^{fr} = 1.8088\omega\mu pa^2L_p \tag{105}$$

Similarly, for the pin side deformational heat generation,

$$Q_{ps}^{def} = 1.8088\omega\tau_{yield}a^2L_p \tag{106}$$

The total heat generation at the pin side is

$$Q_{ps} = 1.8088\omega\mu pa^2L_p(1-\delta_{ps}) + 1.8088\omega\tau_{yield}a^2L_p\delta_{ps} \tag{107}$$

and

$$Q_{ps\eta} = 1.8088\eta_{fd}\omega a^2L_p\left[\mu p(1-\delta_{ps}) + \tau_{yield}\delta_{ps}\right] \tag{108}$$

Then the total heat generation for the pentagonal profile pin with flat shoulder is given as

$$Q_{total} = \eta_{fd}\omega\begin{bmatrix} \frac{2}{3}\pi\mu p\left(R_s^3 - 0.6155a^3\right)(1-\delta_{st}) + \frac{2}{3}\pi\tau_{yield}\left(R_s^3 - 0.6155a^3\right) \\ + \frac{2}{3}\pi\mu p(0.6155a^3)(1-\delta_{pt}) + \frac{2}{3}\pi\tau_{yield}(0.6155a^3)\delta_{pt} \\ + 1.8088\eta_{fd}a^2L_p\left[\mu p(1-\delta_{ps}) + \tau_{yield}\delta_{ps}\right] \end{bmatrix} \tag{109}$$

Fraction of heat generation at the shoulder

$$f_s = \frac{Q_{st}}{Q_{total}} = \frac{\frac{2}{3}\pi\mu p\left(R_s^3 - 0.6155a^3\right)(1-\delta_{st}) + \frac{2}{3}\pi\tau_{yield}\left(R_s^3 - 0.6155a^3\right)}{\begin{bmatrix} \frac{2}{3}\pi\mu p\left(R_s^3 - 0.6155a^3\right)(1-\delta_{st}) + \frac{2}{3}\pi\tau_{yield}\left(R_s^3 - 0.6155a^3\right) \\ + \frac{2}{3}\pi\mu p(0.6155a^3)(1-\delta_{pt}) + \frac{2}{3}\pi\tau_{yield}(0.6155a^3)\delta_{pt} \\ + 1.8088\eta_{fd}a^2L_p\left[\mu p(1-\delta_{ps}) + \tau_{yield}\delta_{ps}\right] \end{bmatrix}} \tag{110}$$

Fraction of heat generation at the pin

$$f_p = \frac{Q_p}{Q_{total}} = \frac{\left\{\begin{array}{l} \frac{2}{3}\pi\mu p(0.6155a^3)(1-\delta_{pt}) + \frac{2}{3}\pi\tau_{yield}(0.6155a^3)\delta_{pt} \\ +1.8088\eta_{fd}a^2L_p\left[\mu p(1-\delta_{ps}) + \tau_{yield}\delta_{ps}\right] \end{array}\right\}}{\left[\begin{array}{l} \frac{2}{3}\pi\mu p\left(R_s^3 - 0.6155a^3\right)(1-\delta_{st}) + \frac{2}{3}\pi\tau_{yield}\left(R_s^3 - 0.6155a^3\right) \\ +\frac{2}{3}\pi\mu p(0.6155a^3)(1-\delta_{pt}) + \frac{2}{3}\pi\tau_{yield}(0.6155a^3)\delta_{pt} \\ +1.8088\eta_{fd}a^2L_p\left[\mu p(1-\delta_{ps}) + \tau_{yield}\delta_{ps}\right] \end{array}\right]} \tag{111}$$

The energy per unit length of the weld for the flat shoulder tool is

$$Q'_{Energy} = \frac{\omega\eta_{fd}}{vR_s^2}\left[\begin{array}{l} \frac{2}{3}\pi\mu F\left(R_s^3 - 0.6155a^3\right)(1-\delta_{st}) + \frac{2}{3}\pi\tau_{yield}A_s\left(R_s^3 - 0.6155a^3\right) \\ +\frac{2}{3}\pi\mu F(0.6155a^3)(1-\delta_{pt}) + \frac{2}{3}\pi A_s\tau_{yield}(0.6155a^3)\delta_{pt} \\ +1.8088\frac{a^2}{\pi}L_p\left[\mu F(1-\delta_{ps}) + A_s\tau_{yield}\delta_{ps}\right] \end{array}\right] \tag{112}$$

While the total heat generation for the pentagonal profile pin with conical shoulder is given as

$$Q_{total} = \eta_{fd}\omega\left\{\begin{array}{l} \frac{2}{3}\pi\omega\left[\begin{array}{l} \mu p\left(R_s^3 - 0.6155a^3\right)(1-\delta_{st})(1+tan\alpha) \\ +\tau_{yield}\left(R_s^3 - 0.6155a^3\right)(1+tan\alpha) \end{array}\right] + \frac{2}{3}\pi\omega\mu p(0.6155a^3)(1-\delta_{pt}) \\ +\frac{2}{3}\pi\omega\tau_{yield}(0.6155a^3)\delta_{pt} + 1.8088\omega a^2L_p\left[\mu p(1-\delta_{ps}) + \tau_{yield}\delta_{ps}\right] \end{array}\right\} \tag{113}$$

Fraction of heat generation at the shoulder

$$f_s = \frac{Q_{st}}{Q_{total}} = \frac{\frac{2}{3}\pi\omega\eta_{fd}\left[\begin{array}{l} \mu p\left(R_s^3 - 0.6155a^3\right)(1-\delta_{st})(1+tan\alpha) \\ +\tau_{yield}\left(R_s^3 - 0.6155a^3\right)(1+tan\alpha) \end{array}\right]}{\left[\begin{array}{l} \frac{2}{3}\pi\omega\eta_{fd}\left[\begin{array}{l} \mu p\left(R_s^3 - 0.6155a^3\right)(1-\delta_{st})(1+tan\alpha) \\ +\tau_{yield}\left(R_s^3 - 0.6155a^3\right)(1+tan\alpha) \end{array}\right] \\ +\frac{2}{3}\pi\omega\mu p(0.6155a^3)(1-\delta_{pt}) + \frac{2}{3}\pi\omega\tau_{yield}(0.6155a^3)\delta_{pt} \\ +1.8088\omega a^2L_p\left[\mu p(1-\delta_{ps}) + \tau_{yield}\delta_{ps}\right] \end{array}\right]} \tag{114}$$

Fraction of heat generation at the pin

$$f_p = \frac{Q_p}{Q_{total}} = \frac{\left[\begin{array}{l} \frac{2}{3}\pi\omega\mu p(0.6155a^3)(1-\delta_{pt}) + \frac{2}{3}\pi\omega\tau_{yield}(0.6155a^3)\delta_{pt} \\ +1.8088\omega\mu p \\ a^2L_p\left[\mu p(1-\delta_{ps}) + \tau_{yield}\delta_{ps}\right] \end{array}\right]}{\left[\begin{array}{l} \frac{2}{3}\pi\omega\eta_{fd}\left[\begin{array}{l} \mu p\left(R_s^3 - 0.6155a^3\right)(1-\delta_{st})(1+tan\alpha) \\ +\tau_{yield}\left(R_s^3 - 0.6155a^3\right)(1+tan\alpha) \end{array}\right] \\ +\frac{2}{3}\pi\omega\mu p(0.6155a^3)(1-\delta_{pt}) + \frac{2}{3}\pi\omega\tau_{yield}(0.6155a^3)\delta_{pt} \\ +1.8088\omega a^2L_p\left[\mu p(1-\delta_{ps}) + \tau_{yield}\delta_{ps}\right] \end{array}\right]} \tag{115}$$

The energy per unit length of the weld for the conical shoulder tool is

$$Q'_{Energy} = \frac{\omega\eta_{fd}}{vR_s^2}\begin{bmatrix} \frac{2}{3}\mu F\left(R_s^3 - 0.6155a^3\right)(1-\delta_{st})\left(1+tan\alpha\right) \\ +\frac{2}{3}A_s\tau_{yield}\left(R_s^3 - 0.6155a^3\right)\left(1+tan\alpha\right) \\ +\frac{2}{3}\mu F(0.6155a^3)(1-\delta_{pt}) + \frac{2}{3}A_s\tau_{yield}(0.6155a^3)\delta_{pt} \\ +1.8088\frac{a^2}{\pi}L_p\left[\mu F(1-\delta_{ps}) + A_s\tau_{yield}\delta_{ps}\right] \end{bmatrix} \tag{116}$$

3.4 Hexagonal pin profile

The tool design for the hexagonal pin is presented in Fig. 7. Deriving the different quantities, the surface under examination is characterized by either being a vertical or horizontal surface.

$$Q_{st}^{fr} = \int_0^{2\pi}\int_0^{R_s} u\,\mu prdrd\theta - 12\int_0^{\frac{\pi}{6}}\int_0^{R_p} u\,\mu prdrd\theta \tag{117}$$

The factor '12' at the second term on the RHS of Equ. (117) denotes the six different regions that form the whole hexagonal surface.

$$Q_{st}^{fr} = \int_0^{2\pi}\int_0^{R_s} \mu p\left(\omega r \pm v_w sin\theta\right)r\;\; drd\theta - 12\int_0^{\frac{\pi}{6}}\int_0^{R_p} \mu pr\left(\omega r \pm v_w sin\theta\right)drd\theta \tag{118}$$

After the integration of Equ. (118) while neglecting the heat generated due to advancing and retracting, gives

$$Q_{st}^{fr} = \frac{2}{3}\pi\omega\mu p\left(R_s^3 - R_p^3\right) \tag{119}$$

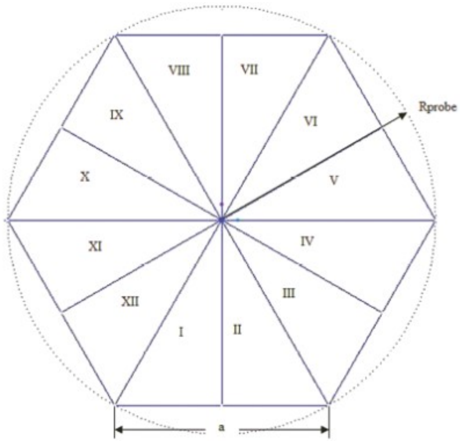

Fig.7. Schematic of the hexagonal pin/probe [8].

But from the geometrical analysis of Fig.7, $R_P = a$

$$Q_{st}^{fr} = \frac{2}{3}\pi\omega\mu p\left(R_s^3 - a^3\right) \tag{120}$$

Similarly, for the shoulder tip deformational heat generation,

$$Q_{st}^{def} = \frac{2}{3}\pi\omega\tau_{yield}\left(R_s^3 - a^3\right) \tag{121}$$

The total heat generation at the shoulder tip is

$$Q_{st} = \frac{2}{3}\pi\omega\mu p\left(R_s^3 - a^3\right)(1-\delta_{st}) + \frac{2}{3}\pi\omega\tau_{yield}\left(R_s^3 - a^3\right) \tag{122}$$

Then

$$Q_{st\eta} = \frac{2}{3}\pi\omega\eta_{fd}\left[\mu p\left(R_s^3 - a^3\right)(1-\delta_{st}) + \tau_{yield}\left(R_s^3 - a^3\right)\right] \tag{123}$$

If the shoulder is conical, then

$$Q_{st\eta} = \frac{2}{3}\pi\omega\eta_{fd}\left[\mu p\left(R_s^3 - a^3\right)(1-\delta_{st})\left(1+tan\alpha\right) + \tau_{yield}\left(R_s^3 - a^3\right)\left(1+tan\alpha\right)\right] \tag{124}$$

The pin tip frictional heat generation is given as

$$Q_{pt}^{fr} = 12\int_0^{\frac{\pi}{6}} \int_0^{R_p} \mu pr\left(\omega r \pm v_w sin\theta\right)drd\theta \tag{125}$$

Which gives Eq.(126) on expansion

$$Q_{pt}^{fr} = 12\mu p\left[\omega\int_0^{\theta=\frac{\pi}{6}} \int_{R_p=0}^{R_p} r^2 drd\theta \pm v_w \int_0^{\theta=\frac{\pi}{6}} \int_{R_p=0}^{R_p} rsin\theta drd\theta\right] \tag{126}$$

On carrying the above integration as shown in Equ. (126), while neglecting the heat generated due to advancing and retracting, gives

$$Q_{st}^{fr} = \frac{2}{3}\pi\omega\mu pa^3 \tag{127}$$

where the geometrical analysis of Fig. 7 shows that $R_P = a$. Similarly, for the pin tip deformational heat generation,

$$Q_{st}^{def} = \frac{2}{3}\pi\omega\tau_{yield}a^3 \tag{128}$$

The total heat generation at the pin tip is

$$Q_{st} = \frac{2}{3}\pi\omega\mu pa^3(1-\delta_{st}) + \frac{2}{3}\pi\omega\tau_{yield}a^3\delta_{st} \tag{129}$$

and

$$Q_{st\eta} = \frac{2}{3}\pi\omega\eta_{fd}\left[\mu pa^3(1-\delta_{pt}) + \tau_{yield}\delta_{pt}a^3\right] \tag{130}$$

The pin side frictional heat generation is given as

$$Q_{ps}^{fr} = 6\int_{R_p=0}^{R_p=a} \int_{L=0}^{L=L_p} \omega r\,\mu prdxdy \tag{131}$$

The factor '6' at the RHS of Equ. (131) denotes the three sides of the hexagonal pin.

$$Q_{ps}^{fr} = 6\int_{R_p=0}^{R_p=a} \int_{L=0}^{L=L_p} \omega r\,\mu prdxdy \tag{132}$$

After substitution of the velocity,

$$Q_{ps}^{fr} = 6\int_{R_p=0}^{R_p=a} \int_{L=0}^{L=L_p} \left(\omega r \pm v_w sin\theta\right)\mu pdxdy \tag{133}$$

Expanding as before,

$$Q_{ps}^{fr} = 6\mu p\left[\omega\int_{R_p=0}^{R_p=a} \int_{L=0}^{L=L_p} rdrdy + v_w \int_{R_p=0}^{R_p=a} \int_{L=0}^{L=L_p} sin\theta drdy\right] \tag{134}$$

The above integration in Equ. (134) gives (while neglecting the heat generated due to advancing and retracting), gives

$$Q_{ps}^{fr} = 3\mu pa^2L_p \tag{135}$$

Similarly, for the pin side deformational heat generation,

$$Q_{ps}^{def} = 3\omega\tau_{yield}a^2L_p \tag{136}$$

The total heat generation at the pin side is

$$Q_{ps} = 3\omega\mu pa^2L_p(1-\delta_{ps}) + 3\omega\tau_{yield}a^2L_p\delta_{ps} \tag{137}$$

and

$$Q_{ps\eta} = 3\eta_{fd}\,\omega\mu pa^2L_p\left[\mu p(1-\delta_{ps}) + \tau_{yield}\delta_{ps}\right] \tag{138}$$

Then the total heat generation for the hexagonal profile pin with flat shoulder is derived at as

$$Q_{total} = \eta_{fd}\,\omega\begin{bmatrix}\frac{2}{3}\pi\mu p\left(R_s^3-a^3\right)(1-\delta_{st}) + \frac{2}{3}\pi\tau_{yield}\left(R_s^3-a^3\right) + \frac{2}{3}\pi\mu pa^3(1-\delta_{pt}) \\ +\frac{2}{3}\pi\tau_{yield}a^3\delta_{pt} + 3\mu pa^2L_p\left[\mu p(1-\delta_{ps}) + \tau_{yield}\delta_{ps}\right]\end{bmatrix} \tag{139}$$

Fraction of heat generation at the shoulder

$$f_s = \frac{Q_{st}}{Q_{total}} = \frac{\frac{2}{3}\pi\mu p\left(R_s^3 - a^3\right)(1-\delta_{st}) + \frac{2}{3}\pi\tau_{yield}\left(R_s^3 - a^3\right)}{\begin{bmatrix} \frac{2}{3}\pi\mu p\left(R_s^3 - a^3\right)(1-\delta_{st}) + \frac{2}{3}\pi\tau_{yield}\left(R_s^3 - a^3\right) + \frac{2}{3}\pi\mu p a^3(1-\delta_{pt}) \\ + \frac{2}{3}\pi\tau_{yield}a^3\delta_{pt} + 3a^2 L_p\left[\mu p(1-\delta_{ps}) + \tau_{yield}\delta_{ps}\right] \end{bmatrix}} \tag{140}$$

Fraction of heat generation at the pin

$$f_p = \frac{Q_p}{Q_{total}} = \frac{\frac{2}{3}\pi\mu p a^3(1-\delta_{pt}) + \frac{2}{3}\pi\tau_{yield}a^3\delta_{pt} + 3\mu p a^2 L_p\left[\mu p(1-\delta_{ps}) + \tau_{yield}\delta_{ps}\right]}{\begin{bmatrix} \frac{2}{3}\pi\mu p\left(R_s^3 - a^3\right)(1-\delta_{st}) + \frac{2}{3}\pi\tau_{yield}\left(R_s^3 - a^3\right) + \frac{2}{3}\pi\mu p a^3(1-\delta_{pt}) \\ + \frac{2}{3}\pi\tau_{yield}a^3\delta_{pt} + 3\mu p a^2 L_p\left[\mu p(1-\delta_{ps}) + \tau_{yield}\delta_{ps}\right] \end{bmatrix}} \tag{141}$$

The energy per unit length of the weld for the conical shoulder tool is

$$Q'_{Energy} = \frac{\omega\eta_{fd}}{vR_s^2}\begin{bmatrix} \frac{2}{3}\left[\mu F\left(R_s^3 - a^3\right)(1-\delta_{st}) + A_s\tau_{yield}\left(R_s^3 - a^3\right)\right] \\ + \frac{2}{3}\mu F a^3(1-\delta_{pt}) + \frac{2}{3}\pi A_s\tau_{yield}a^3\delta_{pt} \\ + 3\frac{a^2}{\pi}L_p\left[\mu F(1-\delta_{ps}) + A_s\tau_{yield}\delta_{ps}\right] \end{bmatrix} \tag{142}$$

While the total heat generation for the hexagonal profile pin with conical shoulder is developed from the above as

$$Q_{total} = \eta_{fd}\,\omega\begin{bmatrix} \frac{2}{3}\pi\left[\mu p\left(R_s^3 - a^3\right)(1-\delta_{st})(1+tan\alpha) + \tau_{yield}\left(R_s^3 - a^3\right)(1+tan\alpha)\right] \\ + \frac{2}{3}\pi\mu p a^3(1-\delta_{pt}) + \frac{2}{3}\pi\tau_{yield}a^3\delta_{pt} + 3a^2 L_p\left[\mu p(1-\delta_{ps}) + \tau_{yield}\delta_{ps}\right] \end{bmatrix} \tag{143}$$

Fraction of heat generation at the shoulder

$$f_s = \frac{Q_{st}}{Q_{total}} = \frac{\frac{2}{3}\pi\left[\mu p\left(R_s^3 - a^3\right)(1-\delta_{st})(1+tan\alpha) + \tau_{yield}\left(R_s^3 - a^3\right)(1+tan\alpha)\right]}{\begin{bmatrix} \frac{2}{3}\pi\left[\mu p\left(R_s^3 - a^3\right)(1-\delta_{st})(1+tan\alpha) + \tau_{yield}\left(R_s^3 - a^3\right)(1+tan\alpha)\right] \\ + \frac{2}{3}\pi\mu p a^3(1-\delta_{pt}) + \frac{2}{3}\pi\tau_{yield}a^3\delta_{pt} + 3a^2 L_p\left[\mu p(1-\delta_{ps}) + \tau_{yield}\delta_{ps}\right] \end{bmatrix}} \tag{144}$$

Fraction of heat generation at the pin

$$f_p = \frac{Q_p}{Q_{total}} = \frac{\frac{2}{3}\pi\mu p a^3(1-\delta_{pt}) + \frac{2}{3}\pi\tau_{yield}a^3\delta_{pt} + 3\mu p a^2 L_p\left[\mu p(1-\delta_{ps}) + \tau_{yield}\delta_{ps}\right]}{\begin{bmatrix} \frac{2}{3}\pi\left[\mu p\left(R_s^3 - a^3\right)(1-\delta_{st})(1+tan\alpha) + \tau_{yield}\left(R_s^3 - a^3\right)(1+tan\alpha)\right] \\ + \frac{2}{3}\pi\mu p a^3(1-\delta_{pt}) + \frac{2}{3}\pi\tau_{yield}a^3\delta_{pt} + 3a^2 L_p\left[\mu p(1-\delta_{ps}) + \tau_{yield}\delta_{ps}\right] \end{bmatrix}} \tag{145}$$

The energy per unit length of the weld for the conical shoulder tool is

$$Q'_{Energy} = \frac{\omega\eta_{fd}}{vR_s^2}\begin{bmatrix} \frac{2}{3}\left[\mu F\left(R_s^3 - a^3\right)(1-\delta_{st})(1+tan\alpha) + A_s\tau_{yield}\left(R_s^3 - a^3\right)(1+tan\alpha)\right] \\ + \frac{2}{3}\mu F a^3(1-\delta_{pt}) + \frac{2}{3}A_s\tau_{yield}a^3\delta_{pt} + 3\frac{a^2}{\pi}L_p\left[\mu F(1-\delta_{ps}) + A_s\tau_{yield}\delta_{ps}\right] \end{bmatrix} \tag{146}$$

4. Results and Discussion

Fig. 8 shows the influence of shoulder radius on the rate of heat generation at the shoulder-workpiece, Aluminum alloys (AA-6061-T6). It could be inferred from the results that the shoulder radius is directly proportional to the total heat generated rate at the interface. i.e. as the shoulder radius increases, the rate at which heat is generated at the interface increases. The same trend was noticed in Fig. 9 and 10 where the total heat generation rate increases with increase in pin length and pin radius. This heat propagates either through conduction in the various parts of the workpiece and the tool as well as through convection to the environment. In addition, higher heat generation due to plastic deformation and smaller interfacial contact area with the workpiece leads to lower frictional heat generation relative to the pin. The failure of friction stir welded joints takes place at the heat-affected zone (HAZ) where the density of the needle-shaped precipitate is less. From the fractional heat generation rate analysis carried out in this study, it is shown that depending on the welding conditions, between 80 to 90% heat is generated at the tool shoulder and the remaining amount at other tool surfaces.

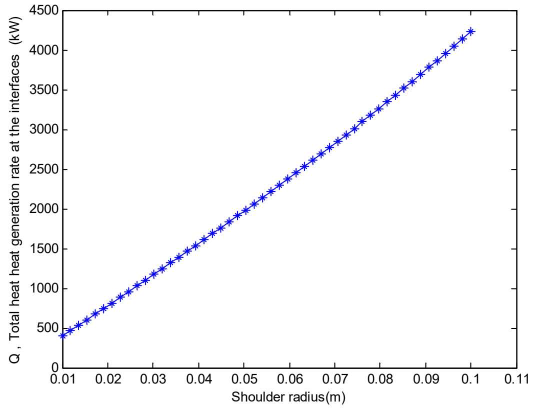

Fig. 8. Variations total heat generation rate at the interfaces with shoulder radius

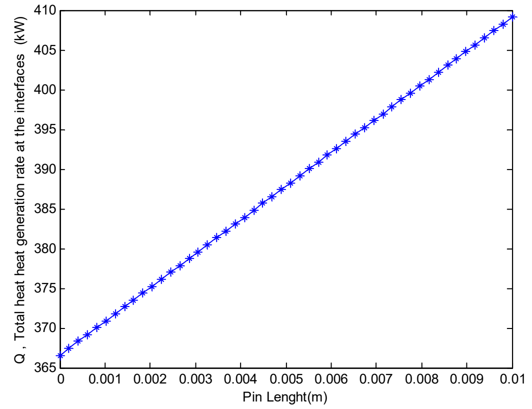

Fig. 9. Variations total heat generation rate at the interfaces with pin length

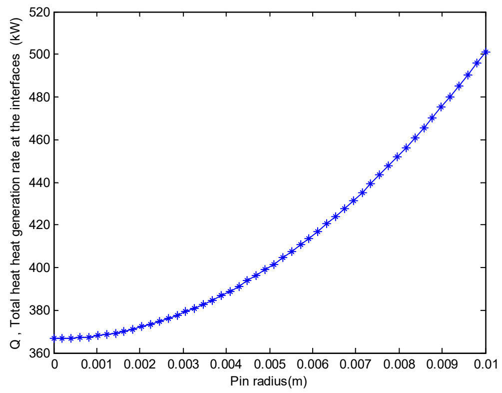

Fig. 10. Variations total heat generation rate at the interfaces with pin radius

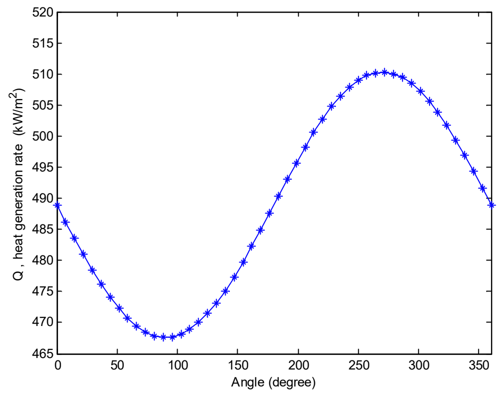

Fig. 11. Variations heat generate with angle of rotation when the extent of sticking is 0.65

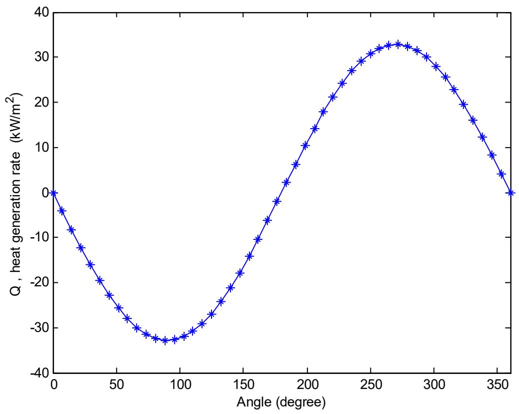

Fig. 12. Variations heat generate with angle of rotation when the extent of sticking is 0 (full sliding condition)

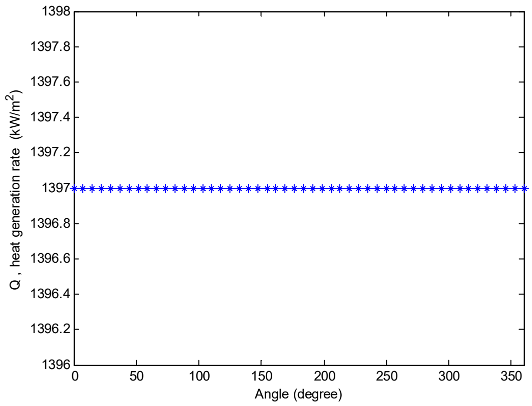

Fig. 13. Variations heat generate with angle of rotation when the extent of sticking is 1 (full sticking condition)

Indisputably, the proportion of the heat generated at the tool shoulder and the pin surfaces is determined by the tool geometry and the welding variables. Also, from the reported literature, it is understood that the pin geometry plays a vital role for material flow, temperature history, grain size, and mechanical properties in the FSW process [8]. Fig. 11 and 12 show the effects of angle of rotation on rate of heat generation when the extent of sticking are 0.65 (sticking and sliding condition) and 1 (full sticking condition). The non-uniformity in the heat generation pattern results from the difference in the relative velocity at different angular locations on the pin surface, which arises due to the variation in term *Usinθ*. The angular variations of temperature on the tool surface results from the local differences in the heat generation rates. Fig. 13 shows the variations of heat generation with angle of rotation when the extent of sticking is 0 (full sliding condition). The result depicts that angle of rotation has no effect on the rate of heat generation when the extent of sticking is 0 as a constant value line is shown in the figure.

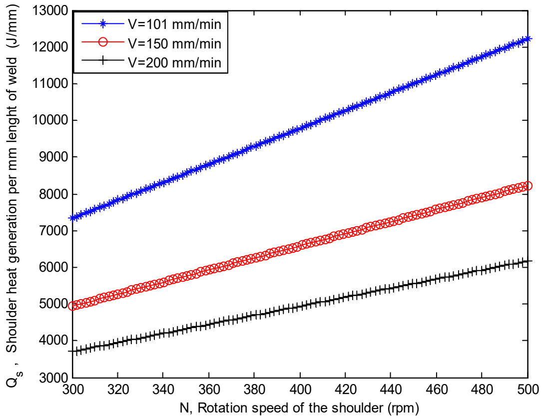

Fig. 14. Effects of welding speed on the heat generation on the heat generation at the shoulder

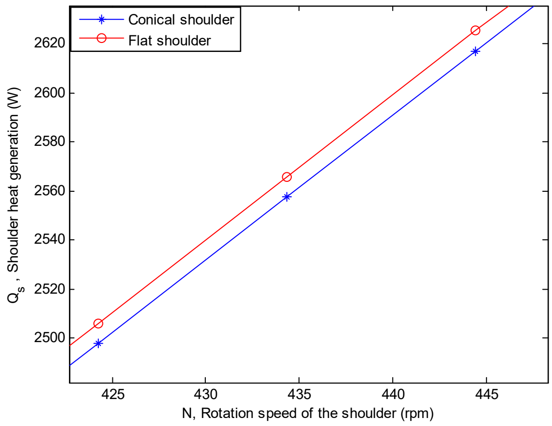

Fig. 15. Effects of shoulder conical angle at the shoulder

Figs. 14-21 present the effects of shoulder rotation speed, conical angle and contact conditions on heat generation. Fig. 14 shows variation of shoulder heat generation rate with welding rotational speed at different welding velocities of 101, 150 and 200 mm/min. while Fig. 15 shows the variation of shoulder heat generation with rotational speed of the shoulder at for conical and flat shoulders. As it could be seen from Fig. 14, the rate of heat generated at the shoulder varies inversely proportional with the welding speed. This is due to the fact that at higher welding velocity, the heat input per unit length decreases as heat is dissipated over a wider region of the workpiece. At high rotational speed, the relative velocity between the tool and workpiece is high, and consequently the heat generation rate and the temperatures are also high.

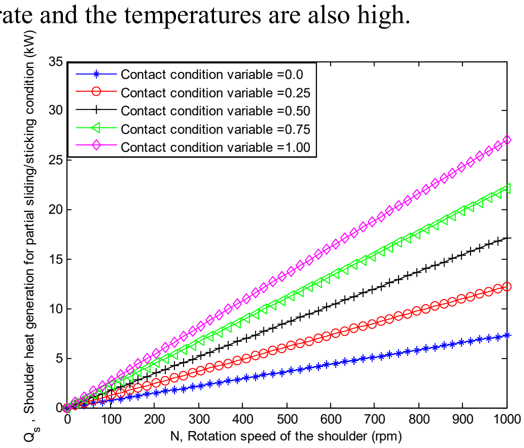

Fig. 16. Effects of contact condition variable on the heat generation at the shoulder

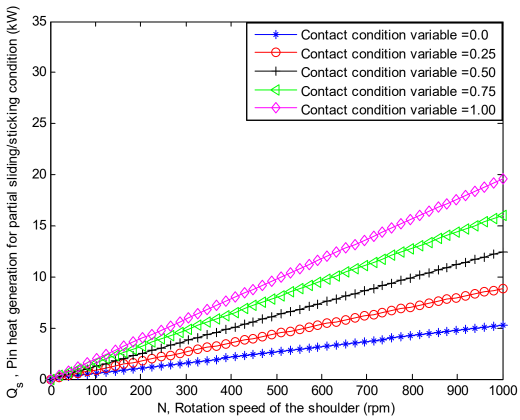

Fig. 17. Effects of contact condition variable on the heat generation at the pin

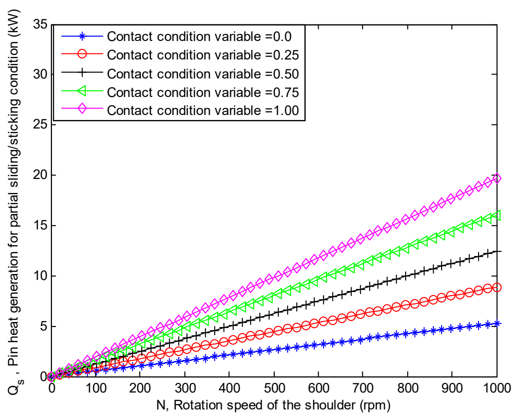

Fig.18. Effects of contact condition variable on the heat generation at the pin

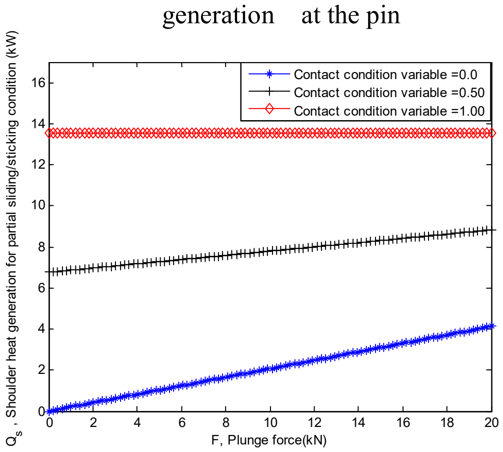

Fig. 19. Effects of contact condition variable on the heat generation at the shoulder with variation of plunge force

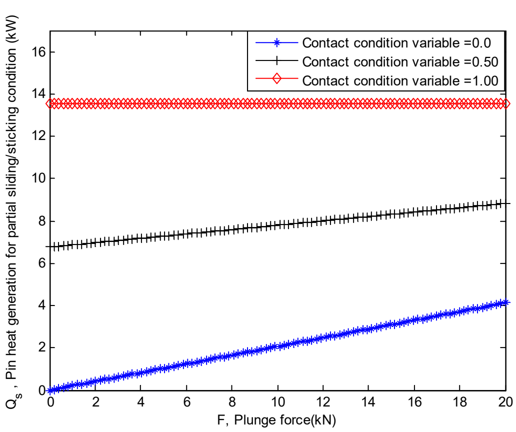

Fig. 20. Effects of contact condition variable on the heat generation at the pin with variation of plunge force

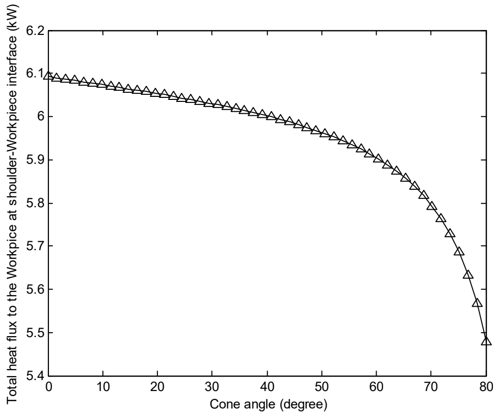

Fig. 21. Effects of conical angle on the heat generation at the shoulder-workpiece interface

The rate of heat generation at the shoulder is more in flat shoulder that the conical shoulder as shown in Fig. 15. This is because the flatness of the shoulder tip increases the tool-workpiece contact surfaces and thereby creating more friction during the process to generate frictional heat and consequently, increases the rate of heat generation. This inference is clearly depicted in Fig.18. The influence of contact condition variables on the rate of heat generation at the shoulder and the pin as displayed in Fig. 16-20. As expected, the heat generation rate increases with the increase in contact condition variables because more heat are generated due to friction due to increased contacts between the tool and the workpiece. Fig. 21 shows the effects of cone angle on the total heat flux on the shoulder-workpiece interface. The figure depicts that the heat flux decreases with the increase in the cone angle. This is because the radius of contact between the shoulder and the workpiece decrease as the conical angle increases and as a result of decrease in the contact radius, the friction between the shoulder-workpiece interface decreases and consequently, the heat generated at the interface decreases.

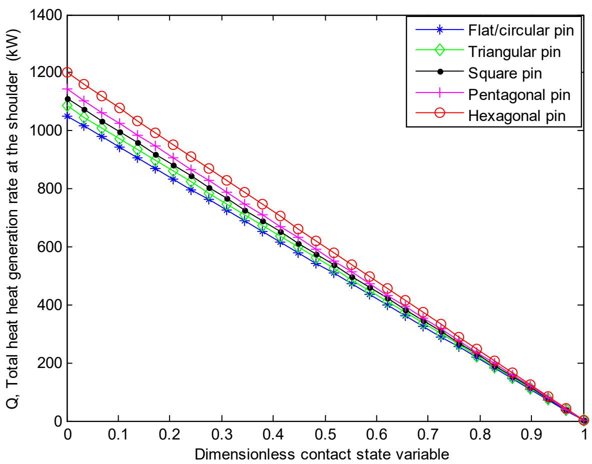

Fig. 22. Effects of pin shape on the total heat generation rate at the interfaces

Fig. 22 shows the effects of tool pin geometry on the total heat generation rate at the interfaces. From the results, the amount of heat generation is directly proportional to the number of edges in the pin profiles in such a way that the heat generated in the profiles increases from the triangular pin profile to hexagonal pin profile. Furthermore, increasing the tool rotational speed under constant weld speed, heat input increases, and increasing the weld speed under constant tool rotational speed, heat input decreases.

For the experimental conditions studied by Ramanjaneyulu *et al.* [25], the results shows that the heat generation and the peak temperature is directly proportional to the number of edges on the pin profile i.e. the heat generation and the peak temperature increase from pin with triangular profile (three edges) to pin with hexagonal profile (six edges). Apart from the fact that our present study establishes this experimental fact analytically, which are not well established by the analytical results of Gadakh *et al.* [8], judging from the established experimental results as stated in the Table, our present study have better predictions for the peak temperature than the previous analytical study as shown in the Table 1. The enhanced predictions are due to the improved models developed in this present work.

Table 1. Comparison of results of heat generated and peak temperature for different tool profiles

Profile	$Q_{Eff,,Energy/ght}$ J/mm[8]	$Q_{Eff,,Energy/ght}$ J/mm (Present study)	T_{max}(K) Experiment [25]	T_{max}(K) Numerical [8]	T_{max} Analytical [8]	T_{max} Analytical (Present study)
Triangle	163.25	393.19	614	733	515	547
Square	167.70	429.64	619	789	516	553
Pentagon	135.63	471.88	623	724	511	559
Hexagon	121.01	514.40	637	713	509	565

5. Conclusion

In this work, improved analytical models have been developed for the predictions of heat generation in straight, tapered/conical shoulder profiles using different pin profiles such as triangular, square, pentagon, and hexagon of the FSW tool. The developed models take into considerations that the welding process is a combination or mixture of the pure sliding and the pure sticking. From the results, it was observed that the amount of heat generation initially increases from the square pin to hexagonal pin profile and then decreases to the triangular pin profile. Furthermore, increasing the tool rotational speed under constant weld speed, heat input increases, and increasing the weld speed under constant tool rotational speed, decreases the heat input and the rate of heat generation at the shoulder is more in flat shoulder that the conical shoulder. The predicted results show good agreements with the experimental results in literature. Therefore, the improved models could be used to estimate the heat generation in FSW tool.

References

1. Thomas W M, Nicholas E D, Needham J C, Murch M G, Temple-Smith P and Dawes C J (1991), *Friction-Stir ButtWelding*, GB Patent No. 9125978.8, International Patent Application No. PCT/ GB92/02203.
2. Schneider J. Temperature distribution and resulting metal flow, friction stir welding and processing, ASM International, Chapter 3, pp. 37–50, 2007
3. Schneider J. A. Temperature Distribution and Resulting Metal Flow. In: Mishra RS, Mahoney MW, editors. Friction Stir Welding and Processing. Materials Park, OH (USA): ASM International; pp. 71-110, 2007
4. Schneider J, Beshears R, Nunes Jr. AC. Interfacial Sticking and Slipping in the Friction Stir Welding Process. Mat SciEng A. Vol. 435 – 436, pp. 297 – 304, 2006
5. Chao, Y. J. Qi, X. Tang, W. Heat transfer in friction stir welding: experimental and numerical studies, ASME J. *Manuf. Sci. Eng*. 125, 138–145, 2003.
6. Frigaard, O., Grong, O., and Midling, O. T. A process model for friction stir welding of age hardening aluminium alloys. Metall. Mater. Trans. A. Vol. 32, pp. 1189–1200, 2001.
7. Russell M J and Shercliff H R 1999 1st Int. Symp. on Friction Stir Welding (Thousand Oaks, California, USA)
8. Gadakh, V. S., Kumar, A and Patil J.V. Analytical Modeling of the Friction Stir Welding Process using Different Pin Profiles. Welding Research. Vol. 94(4): pp. 115-124, 2015.
9. Colegrove, P.A., Shercliff, H.R., Zettler, R., A model for predicting the heat generation and temperature in friction stir welding from the material properties. Sci. Technol. Weld. Joining, Vol.12, pp. 284–297, 2007.
10. Djurdjanović, M., et al., Heat Generation During Friction Stir Welding Process, Tribology in Industry, Vol. 31(1-2), pp. 8-14, 2009.
11. Mijajlović, M., and Milčić, D. Analytical model for estimating the amount of heat generated during friction stir welding: Application on plates made of aluminium alloy 2024-T351, pp. 247–274, 2012.
12. Jauhari TK. Development of Multi-Component Device for Load Measurement and Temperature Profile for Friction Stir Welding Process [M.Sc Thesis]. Penang: Universiti Sains Malaysia; Unpublished. 2012.
13. Arora A, Nandan R, Reynolds AP, Debroy T. Torque, power requirement and stir zone geometry in friction stir welding through modeling and experiments. Scripta Mater Vol. 60, pp. 13–16, 2009.
14. El-Tayeb NSM, Low KO, Brevern PV. On the surface and tribological characteristics of burnished cylindrical Al-6061. Tribol. Int Vol. 42, pp. 320–326, 2009.
15. Devaraju A, Kumar A, Kotiveerachari B. Influence of addition of Grp/Al2O3p with SiCp on wear properties of aluminum alloy 6061-T6 hybrid composites via friction stir processing. Trans Nonferrous Met Soc China, Vol. 23, pp. 1275–1280, 2013.

16. Sheppard T. and D. Wright D. Determination of flow stress. Part 1 constitutive equation for aluminum alloys at elevated temperatures, Met. Technol., Vol. 6, pp. 215–223, 1979.
17. Sheppard, T., A Jackson . "Constitutive equations for use in prediction of flow stress during extrusion of aluminium alloys", Materials Science and Technology, Vol 13(3), pp. 203–209.
18. Uyyuru RK, Kallas SV. Numerical analysis of friction stirs welding process. J Mater Eng Perform 15:505–18, 2006.
19. Colegrove, P.A., Shercliff, H.R.. CFD Modelling of the friction stir welding of thick Plate 7449 aluminium alloy. Sci. Technol. Weld. Joining Vol. 11 (4), pp. 429–441, 2006.
20. Wang H, Colegrove PA, Dos Santos JF. Numerical investigation of the tool contact condition during friction stir welding of aerospace aluminium alloy. Comput Mater Sci.; Vol. 7, pp. 101–108, 2013.
21. Su H, Wu C, Chen M. Analysis of material flow and heat transfer in friction stir welding of aluminium alloys. China Weld (Engl Ed), Vol. 22, pp. 6–10, 2013.
22. Sobamowo, M. G. New models for the prediction of temperature-strain dependent flow stress during machining and fabrication of material. Report on Improved models for flow stress predictions. Unpublished Work, 2016.
23. Schmidt, H., Hattel, J., and Wert, J. An analytical model for the heat generation in friction stir welding. *Modelling Simul. Mater. Sci. Eng. Vol.* 12: 143–157, 2004.
24. Khandkar, M. Z. H., Khan, J. A., and Reynolds, A. P. Prediction to temperature distribution and thermal history during friction stir welding: Input torque basedmodel. *Sci. Technol. Weld. Join. Vol.* 8, pp. 165–174, 2003.
25. Ramanjaneyulu, K., Reddy, G. M., Venugopal, A. V. and Markandeya, R. Structure-Property Correlation of AA2014 Friction Stir Welds: Role of Tool Pin Profile. Journal of Materials Engineering and Performance, Vol. 22(8), pp. 2013-2225, 2013.